AD-A114 777 PENNSYLVANIA STATE UNIV UNIVERSITY PARK APPLIED RESE--ETC F/G 20/1
EXPERIMENTAL METHOD TO MEASURE LOW FREQUENCY SOUND RADIATION - --ETC(U)
FEB 82 W Y STRONG N00024-79-C-6043
UNCLASSIFIED ARL/PSU/TM-82-71 NL

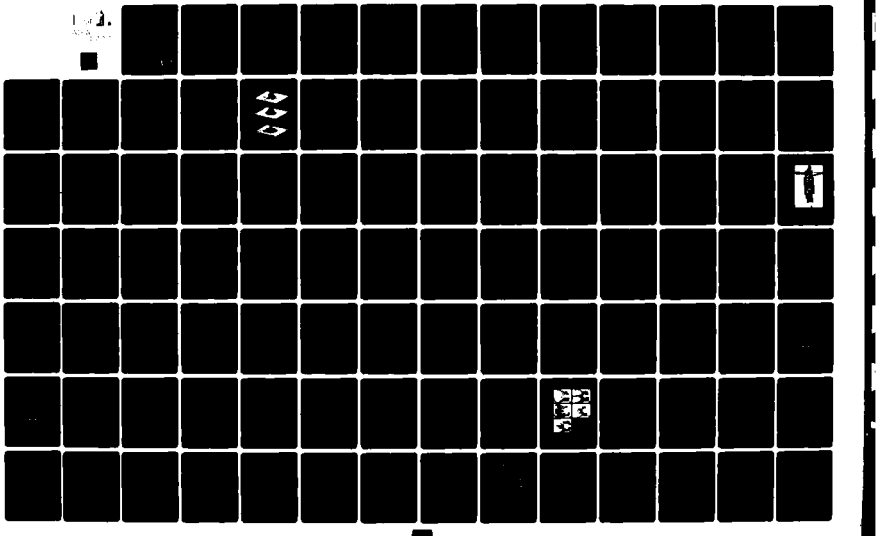

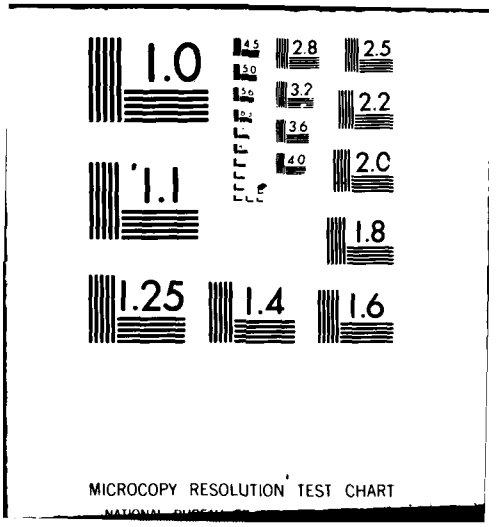
1.0
1.1
1.25
1.4
1.6
1.8
2.0
2.2
2.5
2.8
3.2
3.6
4.0
4.5
5.0
5.6
6.3
MICROCOPY RESOLUTION TEST CHART

(6)

EXPERIMENTAL METHOD TO MEASURE LOW FREQUENCY SOUND RADIATION - NEARFIELD ACOUSTICAL HOLOGRAPHY

William Y. Strong, Jr.

Technical Memorandum
File No. TM 82-71
February 3, 1982
Contract No. N00024-79-C-6043

Copy No. 5

The Pennsylvania State University
Intercollege Research Programs and Facilities
APPLIED RESEARCH LABORATORY
Post Office Box 30
State College, PA 16801

NAVY DEPARTMENT

NAVAL SEA SYSTEMS COMMAND

UNCLASSIFIED
SECURITY CLASSIFICATION OF THIS PAGE (When Data Entered)

REPORT DOCUMENTATION PAGE		READ INSTRUCTIONS BEFORE COMPLETING FORM
1. REPORT NUMBER TM 82-71	2. GOVT ACCESSION NO. AD-A124 777	3. RECIPIENT'S CATALOG NUMBER
4. TITLE (and Subtitle) EXPERIMENTAL METHOD TO MEASURE LOW FREQUENCY SOUND RADIATION - NEARFIELD ACOUSTICAL HOLOGRAPHY		5. TYPE OF REPORT & PERIOD COVERED M.S. Thesis, May 1982 6. PERFORMING ORG. REPORT NUMBER TM 82-71
7. AUTHOR(s) William Y. Strong, Jr.		8. CONTRACT OR GRANT NUMBER(s) N00024-79-C-6043
9. PERFORMING ORGANIZATION NAME AND ADDRESS The Pennsylvania State University Applied Research Laboratory, P. O. Box 30 State College, PA 16801		10. PROGRAM ELEMENT, PROJECT, TASK AREA & WORK UNIT NUMBERS
11. CONTROLLING OFFICE NAME AND ADDRESS Naval Sea Systems Command Department of the Navy Washington, DC 20362		12. REPORT DATE February 3, 1982 13. NUMBER OF PAGES 94 pages & figures
14. MONITORING AGENCY NAME & ADDRESS(if different from Controlling Office)		15. SECURITY CLASS. (of this report) Unclassified, Unlimited 15a. DECLASSIFICATION/DOWNGRADING SCHEDULE

16. DISTRIBUTION STATEMENT (of this Report)

Approved for public release, distribution unlimited, per NSSC (Naval Sea Systems Command), 6/23/81.

17. DISTRIBUTION STATEMENT (of the abstract entered in Block 20, if different from Report)

18. SUPPLEMENTARY NOTES

19. KEY WORDS (Continue on reverse side if necessary and identify by block number)

thesis, near field, acoustic, holography

20. ABSTRACT (Continue on reverse side if necessary and identify by block number)

A technique called Nearfield Acoustical Holography (NAH) has been developed at The Pennsylvania State University. The technique, a significant improvement over conventional holography, is not subject to the wavelength resolution limitation associated with conventional techniques. An exact formulation of the Green's function propagator allows reconstructions of the entire pressure, particle velocity, and vector intensity fields. The vector intensity may be plotted to show the flow of acoustic energy around and away from a source. On some sources, these mappings reveal areas of non-radiating, circulating energy

DD FORM 1 JAN 73 1473 EDITION OF 1 NOV 65 IS OBSOLETE UNCLASSIFIED

SECURITY CLASSIFICATION OF THIS PAGE (When Data Entered)

20. flow. These areas may have large pressure or velocity amplitudes and negative intensity regions that previously led to misconceptions about the production of acoustic energy.

This work presents details of the development of the NAH system. Included are a review of the theory, details of the experimental apparatus design, accuracy verification, and the use of the system to study a relatively simple source (a homogeneous rectangular plate) and a complex source (an intact, string excited guitar). The guitar research revealed some interesting results such as: the rose is an important source of low frequency energy, the motion of the back plate is very important, and similar plate modes occur at different frequencies due to a complex relationship among the strings, ribs, body, and neck.

ABSTRACT

A technique called Nearfield Acoustical Holography (NAH) has been developed at the Pennsylvania State University. The technique, a significant improvement over conventional holography, is not subject to the wavelength resolution limitation associated with conventional techniques. An exact formulation of the Green's function propagator allows reconstructions of the entire pressure, particle velocity, and vector intensity fields. The vector intensity may be plotted to show the flow of acoustic energy around and away from a source. On some sources, these mappings reveal areas of non-radiating, circulating energy flow. These areas may have large pressure or velocity amplitudes and negative intensity regions that previously led to misconceptions about the production of acoustic energy.

This work presents details of the development of the NAH system. Included are a review of the theory, details of the experimental apparatus design, accuracy verification, and the use of the system to study a relatively simple source (a homogeneous rectangular plate) and a complex source (an intact, string excited guitar). The guitar research revealed some interesting results such as: the rose is an important source of low frequency energy, the motion of the back plate is very important, and similar plate modes occur at different frequencies due to a complex relationship among the strings, ribs, body, and neck.

TABLE OF CONTENTS

LIST OF FIGURES

ACKNOWLEDGMENTS

I would like to thank Dr. Julian Maynard, my thesis advisor, for his tireless efforts and support throughout the duration of this work. I would also like to thank Dr. Earl Williams, a friend and a gifted researcher, for his constant help and inspiration. He may well have taught me more about acoustics, and myself, than anyone else during my graduate studies. Lastly, I would like to thank my comrades, Todd Beyer, a friend who I worked quite closely with during the construction and de-bugging of the holographic system, and Don Bowen, a meticulous keeper of order and fellow team member. Without these people, surely this work would not have been possible. The Applied Research Laboratory was invaluable to this work in its provision of materials and expert shop facillities.

This work was funded by The Applied Research Laboratory at The Pennsylvania State University under contract with the Naval Sea Systems Command.

CHAPTER ONE

INTRODUCTION

1.1 Statement of the Problem

Mechanical vibrators and their radiated sound fields have been of considerable interest in the past. Yet how the motion of the vibrator couples to the medium to produce sound and how this sound energy flows away from the vibrator to the farfield remains inadequately understood. Mathematical predictions of the sound field produced by a vibrator are quite involved and only a few idealized sources may be studied in this manner. The mathematics necessary for studying a complex vibrator exceed the realm of practical solution. Consequently, experimental methods have been pursued to study complex vibrators. Many existing measurement techniques accurately record the properties that they were designed to measure, but the information provided to the researcher does not reveal the total radiation picture. For obvious academic and practical reasons, it would be advantageous to develop better experimental techniques and expand our understanding of the relationship between a complex vibrator and its radiated sound field.

The purpose of this work is to present a new technique called Nearfield Acoustical Holography that has many distinct advantages over other techniques for sound radiation measurement. This thesis will cover the design and construction of the experimental apparatus, accuracy

checks on the system, and the use of the system with a simple and a complex vibrator.

Nearfield acoustical holography is similar to conventional acoustical holography but an important distinction allows much more information to be obtained from the measurement. This will be discussed in detail later. One important result from this technique is an energy flow map that shows the actual magnitude and direction of the acoustic energy flow field. These flow maps indicate which areas on a vibrator are producing and absorbing energy and also reveal regions of circulating energy flow.

Before describing the differences between nearfield and conventional acoustical holography, a discussion of the basic problem is in order. One would like to be able to correlate the mechanical properties of a complex vibrator with the radiated sound field it produces. This is not an easy connection to make. Exact mathematical solutions that predict the radiated sound field are available for only a few simple sources. If the source is not homogeneous, as in the case of a plate with stiffening rib, then the precise calculation of the sound radiation becomes extremely difficult, if not impossible. The next best solution may be to experimentally study the source using conventional acoustic measuring techniques. But these measurements may be misleading. Take as an example two plates vibrating in some natural mode with one of the plates above coincidence

and the other below coincidence. Measuring both plates with an accelerometer may reveal similar surface velocities in both plates, but the plate operating below coincidence will not radiate much energy into the farfield. The plate operating above coincidence, though it has roughly the same velocity, radiates a larger amount of energy into the farfield. Thus a knowledge of the surface displacement or particle velocity around the vibrator does not necessarily determine how sound energy is transmitted to the sound field. In general, the problem is not so severe at higher frequencies, above coincidence, where large surface displacements most likely produce the radiated energy. The difficulty occurs at lower frequencies where the radiated wavelength is larger than the source dimensions. At lower frequencies large displacements or pressure amplitudes may actually correspond to sinks of acoustic energy.

To accurately determine how a vibrator radiates sound and how this energy flows into the farfield, a knowledge of the acoustic intensity vector field is required. This is defined as a product of the in-phase components of the pressure and the particle velocity, i.e.

$$\vec{I}(\vec{r}) = 1/2\ p(\vec{r})\ \vec{v}(\vec{r})\ \cos\theta(\vec{r}) \qquad (1)$$

where θ is the phase difference between the pressure and the velocity. Since this is a vector it gives the rate and direction of the acoustic energy flow at any point in space. A large component of this quantity normal to the vibrator

corresponds to an energy-producing area on the vibrator. Because of this, interest in measuring $\bar{I}(r)$ has recently grown. A two-microphone technique for measuring intensity is available, but it is limited in that it records only one component of the intensity at one point. This limited data can lead to confusion in defining the energy-producing regions that radiate to the farfield because of the existence of non-radiating, circulating intensity fields. Using the two-microphone technique to map a sufficiently large energy flow field would be quite time consuming.

The following is a list of some of the important features of nearfield acoustical holography[1]:

1. One non-contact measurement allows analysis of the entire sound field above the vibrator.

2. Data taking is accomplished quickly, requiring roughly 15 minutes from beginning of the data aquisition to analyzing the results. This allows the researcher more time to study the results rather than record data.

3. The measurement area is large so that sources can be pinpointed within roughly a 10 m^2 area.

4. The measurement area subtends a large solid angle from the source and therefore can measure multi-directional sources without missing information.

5. High spatial resolution permits localization of

sources to within about 10 cm.

6. Output can be computer graphic displays of the:

a. sound pressure field from the source farfield,

b. particle velocity field from source to farfield,

c. modal structure of the vibrating surface (obtained from the normal velocity at the source surface),

d. vector intensity field - this locates sources of sound energy and maps the energy flow through the sound field,

e. farfield radiation pattern,

f. total power radiated into the half-space.

Nearfield holography is based on conventional holographic theory. The assumption is that a group of localized sources produces a wave field in three dimensions. This wave field is then measured across a two-dimensional surface. The amplitude and phase information recorded in two dimensions is used to reconstruct the wave field throughout the entire half-space located above the sources. This can be done because the field obeys the acoustic wave equation and Green's theorem applies. The process just described is exact in theory, but in practice, conventional holography poses some severe restrictions on the reconstructed data. In particular, spatial resolution is usually limited by the

radiated wavelength. In other words, details of a source located less than a wavelength apart cannot be resolved and these features appear smoothed out. This makes the detailed study of sound radiation from sources operating at low frequencies unfeasible with conventional acoustical holography. Conventional techniques are also limited to reconstructing a scalar 'intensity' proportional to the square of the pressure. It is not possible to determine the vector intensity, and therefore one cannot pinpoint energy sources or construct energy flow maps. These limitations are due to experimental restrictions that are always present in optical holography but do not necessarily apply to measurements of sound waves. Nearfield holography removes these experimental limitations.

The sound field generated by any monochromatic source can be decomposed into an angular spectrum representing plane waves moving in different directions. Actually, the field is composed of propagating plane waves and evanescent waves. Evanescent waves are those whose amplitudes decrease exponentially with distance from the source. This decay is very rapid, with amplitudes typically 100dB down in just one or two wavelengths from the source. This is well below the dynamic range of most measuring instruments. Conventional holographic techniques measure the wave field at distances of many wavelengths from the source and therefore can not record the evanescent wave information. The propagating plane waves that can be recorded are produced by features of

the source that vary in space with a scale of length that is greater than the radiated wavelength and this results in spatial resolution limitations. Evanescent waves vary in space with a scale of length that is less than the radiated wavelength and, if measured, allow details of the source to be resolved regardless of the size of the radiated wavelength. From a mathematical point of view, the evanescent wave information is needed for the exact application of Green's theorem. An example of the dramatic effects of the evanescent wave components is illustrated in Fig.1 (Taken from Williams and Maynard, Ref. 4) which shows various aspects of a wave field generated by two simple, experimental sources. Fig.1a shows the pressure field in a plane very close (1/15 of a wavelength) to the plane of the sources. Even this close there is very little information that would indicate two distinct sources. Fig.1b, the reconstructed pressure using conventional holography, shows the effect of leaving out the evanescent wave information. The details of the two sources have been smoothed over a wavelength and any indication as to the location and number of sources is lost. Fig.1c shows the reconstruction that retains the evanescent information. The sources can be clearly resolved.

Nearfield holography strives to measure as much of the evanescent wave information as possible by using an instrument with a large dynamic range, and, since the evanescent waves decay exponentially with distance from the

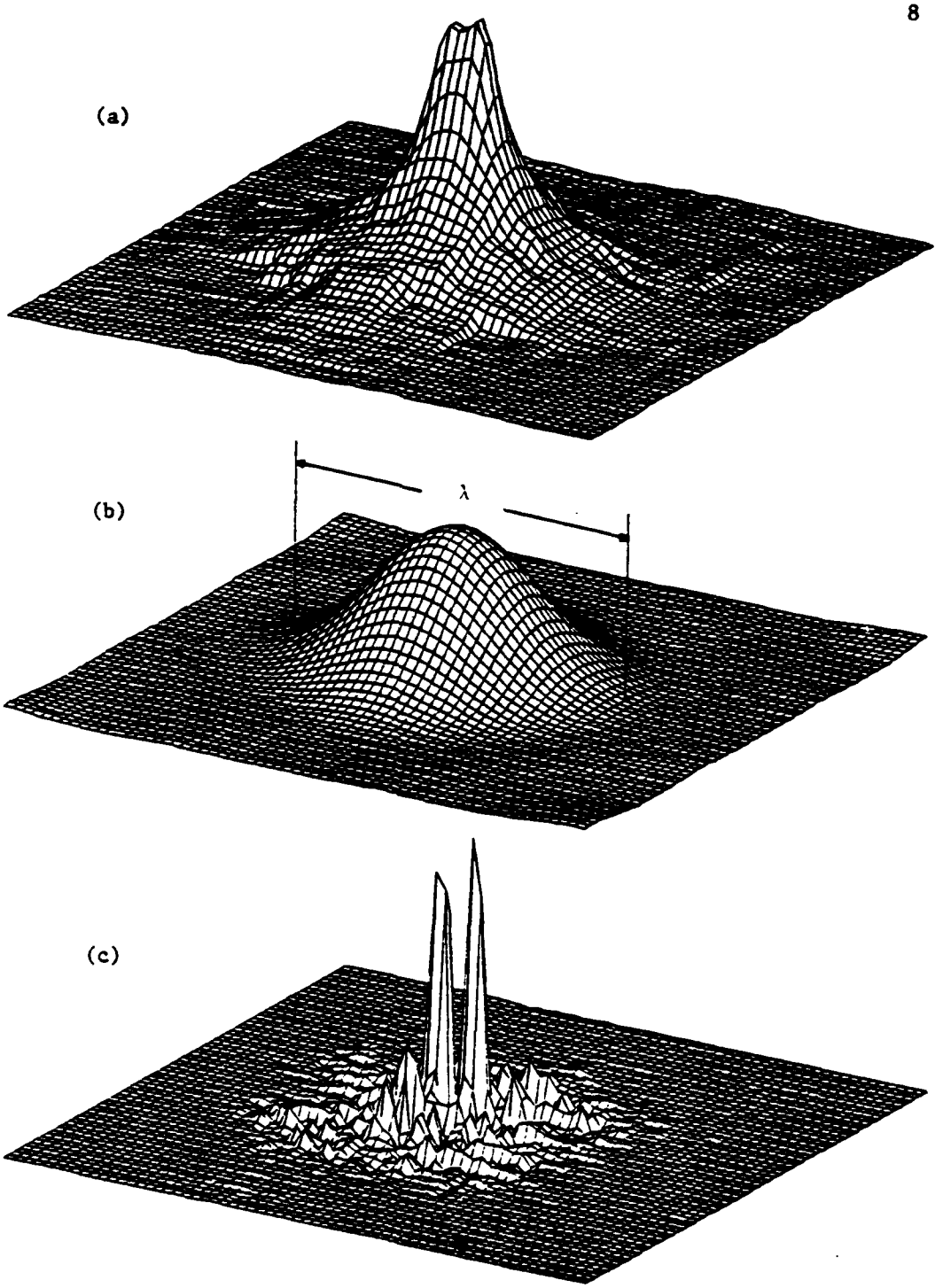

Figure 1. Holographic Data for Two Point Sources. (a) Sound-Pressure Amplitude in the Hologram Plane. (b) Conventional Holographic Reconstruction of the Sources. The Resolution-Limiting Wavelength is Shown. (c) Reconstruction of the Source Intensity Using Nearfield Holography. The Two Point Sources are Clearly Resolved.

source, the wave field should be measured as close as possible to the source. Once this is done, the evanescent as well as propagating wave information can be recorded and digitally processed with an exact formulation of Green's theorem. This solution seems quite elementary and the question may arise as to why this was not done previously. The reason seems to be that acoustical holography was developed from the technology of optical holography where it is impossible to measure evanescent waves due to the very small optical wavelengths. In low frequency sound fields it is easy to make measurements within a wavelength from the source since acoustic wavelengths can be a meter or more, but there was no motivation from optical holography to do so. Additionally, it is not obvious that measuring the nearfield pressure alone is enough to characterize how a source delivers acoustic energy to a medium. The nearfield pressure (or particle velocity) alone is not enough to determine how a vibrator radiates sound; the complete vector intensity is required to do this. If nearfield measurements are made, an exact form of Green's theorem allows one to calculate the velocity field from the pressure field and then obtain the vector intensity from these two. In fact, any desired property of the entire sound field may be calculated with this technique. Omitting the evanescent waves precludes exact calculations and therefore one is left with the limits of conventional holography. Fortunately, a large class of radiators can be measured using nearfield

holography and a great deal of new information becomes available.

1.2 Discussion of Theory

An overview of the mathematical theory used in nearfield holography is in order[2]. This discussion will be limited to single frequency, planar sources and a time dependence of exp(-iwt) is assumed. The fundamental equations make use of Green's theorem which states that a knowledge of the complex pressure, representing amplitude and phase, across an infinite plane located in a sound field allows one to propagate to any other parallel plane and determine exactly the complex pressure there. The relationship expressing this is Rayleigh's second integral:

$$p(x,y,z)=C\iint_{-\infty}^{\infty} p(x',y',d)\{\partial/\partial z'[\exp(ikR)/R]_{|z'=d}\}dx'dy' \quad (2)$$

where $p(x',y',d)$ = the pressure in a source plane located at $z' = d$

$p(x,y,z)$ = the pressure in a plane z away from the source plane

$\partial/\partial z'[\exp(ikR)/R]_{|z'=d}$ = pressure-pressure Green's function

$$R = \sqrt{(x-x')^2+(y-y')^2+(z-z')^2}$$

$$C = (-1/2\pi)$$

$$\pi = 3.1416$$

and $z \geq z'$

This equation allows us to determine the pressure at a distance z from the source. But we would like to be able to

measure the pressure in a plane at some distance z=h (hologram plane) and use the mathematics to propagate back to the source plane at z=d. To do this, we rewrite equation (2) as:

$$p(x,y,z) = \iint_{-\infty}^{\infty} p(x',y',d)\, g(x-x',y-y',z-d)\, dx'\, dy' \qquad (3)$$

$$\text{where } g(x-x',y-y',z-d) = C\, \partial/\partial z' [\exp(ikR)/R]_{|z'=d}$$

This form is recognizable as a two-dimensional convolution integral that may be written as:

$$p(x,y,z) = p(x',y',d) * g(x-x',y-y',z-d) \qquad (4)$$

where * denotes the convolution operation. The convolution integral itself is quite difficult, but by employing Fourier transform techniques, we can transform the equation into frequency space. Once this is done, the convolution becomes a simple product of two terms. Once the product is formed, the inverse Fourier transform returns the relation to real-space.

The two-dimensional Fourier transform may be defined as:

$$P(k_x,k_y,d) \equiv \iint_{-\infty}^{\infty} p(x,y,d)\exp(-ik_x x)\exp(-ik_y y)\,dx\,dy \qquad (5)$$

If we transform both sides of equation (4) we have:

$$P(k_x,k_y,z) = P(k_x,k_y,d)\, G(k_x,k_y,z-d) \qquad (6)$$

$$\text{where } G = C\, F\{\partial/\partial z' [\exp(ikR)/R]_{|z'=d}\}$$

and F denotes the Fourier transform operation.

Since the two-dimensional transform does not operate on z', G may be rewritten as:

$$G = C\ \partial/\partial z' \{F[\exp(ikR)/R]\}_{|z'=d} \tag{7}$$

With some work, the transform of the Green's function is found to be:

$$F[\exp(ikR)/R] = \frac{\exp(iz\sqrt{k^2 - k_x^2 - k_y^2})}{i\sqrt{k^2 - k_x^2 - k_y^2}} \tag{8}$$

where $k = 2\pi/\lambda = 2\pi f/c$
k_x and k_y are spatial frequencies in the x and y directions

If we define $k_z = \sqrt{k^2 - k_x^2 - k_y^2}$, equation (8) becomes:

$$F[\exp(ikR)/R] = \exp(ik_z(z-d))/ik_z$$

After taking the derivative, the transformed Green's function is:

$$G = \exp(i\ k_z\ (z-d))$$

and the final form of equation (6) is:

$$P(k_x,k_y,z) = P(k_x,k_y,d)\ \exp[ik_z(z-d)] \tag{9}$$

Equation (9) also shows the effect of the spatial frequencies on the argument of the exponential. There are two cases:

1. $k_z = \sqrt{k^2-k_x^2-k_y^2}$, for $k^2 \geq k_x^2 + k_y^2$
   such that $G = \exp[i(z-d)\sqrt{k^2-k_x^2-k_y^2}]$

2. $k_z = i\sqrt{k_x^2+k_y^2-k^2}$, for $k^2 < k_x^2 + k_y^2$
   such that $G = \exp[-(z-d)\sqrt{k_x^2+k_y^2-k^2}]$

The first case represents the propagating plane waves whose phases change with distance from the source. The second case shows an exponentially decaying function representing the evanescent waves. The function decays rapidly with distance and suggests that measurement of the evanescent waves must be made very close to the source. Inverting equation (9) yields:

$$P(k_x,k_y,d) = P(k_x,k_y,z) \exp[-i\, k_z\, (z-d)] \qquad (10)$$

Equation (10) allows us to measure the pressure in some plane above a source and 'back-propagate' that information to the source plane located at z=d. The inverse Fourier transform of equation (10) returns the information to real space:

$$F^{-1}\,[\,P(k_x,k_y,d)\,] = F^{-1}\,\{\,P(k_x,k_y,z) \exp[-i\, k_z\, (z-d)]\}$$

$$p(x,y,d) = C^2 \iint_{-\infty}^{\infty} P(k_x,k_y,z) \exp[-i\, k_z\, (z-d)] * \exp(ik_x x) \exp(ik_y y)\, dk_x dk_y \qquad (11)$$

Equation (11) is the fundamental relationship of nearfield acoustical holography. It should be noted that d is not restricted to the source plane. In fact, it may correspond to any plane above the source plane. This allows us to

determine the pressure at any point in the half-space located above a source.

The vector velocity which is necessary for calculating the vector intensity may be obtained by considering that the velocity is proportional to the gradient of the pressure, i.e.

$$\vec{\nabla} p = i\,\omega\rho\,\vec{v} \tag{12}$$

where $\vec{\nabla} = [\hat{e}_x\,\partial/\partial x + \hat{e}_y\,\partial/\partial y + \hat{e}_z\,\partial/\partial z]$

The Fourier transform of equation (12) yields:

$$V(k_x,k_y,d) = (1/\omega\rho)[k_x\hat{e}_x + k_y\hat{e}_y - i\hat{e}_z\,\partial/\partial z]\;P(k_x,k_y,d)$$

$$= (1/\omega\rho)[k_x\hat{e}_x + k_y\hat{e}_y + k_z\hat{e}_z\,]\;P(k_x,k_y,z) * \exp[-i\,k_z\,(z-d)] \tag{13}$$

The vector velocity is then obtained by inverse Fourier transforming equation (13):

$$v(x,y,d) = -C/\omega\rho \iint_{-\infty}^{\infty} [k_x\hat{e}_x + k_y\hat{e}_y + k_z\hat{e}_z]\;P(k_x,k_y,z) * \exp[-i\,k_z\,(z-d)] * \exp(ik_x x)\,\exp(ik_y y)\,dk_x\,dk_y \tag{14}$$

It should again be noted that z is not restricted to the source plane (z=d) and may correspond to any plane above the source. The modal structure of the vibrator may be obtained by considering the normal component of the velocity at the surface of the source. From equation (14), the normal

component is:

$$v(x,y,d) = -C/\omega\rho \iint_{-\infty}^{\infty} k_z \, P(k_x,k_y,z) \exp[-ik_z(z-d)] * \exp(ik_x x) \exp(ik_y y) \, dk_x \, dk_y \qquad (15)$$

The addition of a time factor $\exp(-iwt)$ allows one to view the motion of the surface through time.

We have derived an expression for the pressure in equation (11) and the vector velocity in equation (15), and it is now possible to calculate the vector intensity, $\vec{I}(\vec{r})$, from equation (1). Since the wave field may be reconstructed in any plane, mappings of the intensity may be produced that show the energy flow around and away from the source.

Other quantities that may be calculated include:

The power radiated into a half-space,

$$W = \iint_{-\infty}^{\infty} \vec{I}(x,y,d) \, \hat{e}_z \, dx \, dy \qquad (16)$$

The radiation efficiency, ,

$$= W / (\rho \, c \, S \, \bar{v}^2)$$

where W = power from an object of surface area S
$\bar{v}$ = average RMS velocity of radiating surface

and the directivity pattern,

$$p(r,\theta,\phi) = i\,\omega\rho\,[\exp(ikR)/R]\;V(k_x,k_y,d) \qquad (17)$$

where V is the transformed normal velocity and the spatial frequencies are:

$$k_x = [2\pi/\lambda]\,\cos\theta\,\sin\phi$$
$$k_y = [2\pi/\lambda]\,\sin\theta\,\sin\phi$$

All of this information may be obtained from one, quick measurement of the pressure amplitude and phase in a plane. The time savings are obvious and a great deal of information becomes easily available to the researcher.

1.3 Brief Description of Measurement Technique

An array of 256 electret microphones are suspended in a flat plane (the hologram plane previously mentioned) and are arranged in a 16 x 16 square grid. These microphones record the sound field within 10 cm of the source plane. The physical spacing between the microphones may be varied to change the resolution of the system. The effective sampling of the sound field is enhanced for steady-state sources by scanning the radiated sound field with the array to fill in points between the physical spacing of the microphones. This is actually done by moving the source on a two-dimensional scanning apparatus, an easier operation than moving the microphone array. The source is usually moved through a 16 point (4x4) square grid. The distance between the scanning grid points is determined as follows:

$d = A/4$, where d = distance between grid points
A = microphone spacing in the array

The result of scanning the sound field is a 64 x 64 array of data points rather than the 16 x 16 points available without scanning.

The microphones are sampled to give a time sequence for each. Each time sequence is Fourier transformed to determine the amplitude and relative phase at each microphone. These values are stored in a complex representation and used with the processing techniques described earlier.

CHAPTER TWO

ARRAY CONSTRUCTION

2.1 Historical Introduction

When this project began, an array system using dynamic microphones had been constructed by Williams et al[3]. This system was used for conventional acoustical holography measurements of steady state sources. Shortly after I began my work, it was discovered that the resolution limit of a wavelength that is usually associated with holography need not apply in some acoustic applications[4]. This new technique, which we call non-wavelength limited acoustical holography or nearfield holography[5], required that the measurement be made quite close to the source. This meant that the measurement plane should typicaliy be within 10 cm (4 in) of the source plane. Much work went into the development of this technique , but the results were not as good as we originally expected they would be. In our search for an explaination, we realized that the problem was not in the theoretical development, but rather in some factors related to the actual physical measurement. First, the sources we study are usually electro-mechanically driven. This sets up a varying magnetic field around the source. The dynamic, or moving coil, microphones nearest the source were being influenced by this field and therefore were inaccurately recording the sound field. Second, the microphones were mounted on 5 cm high by .95 cm wide (2 in

by 3/8 in) aluminum beams. The reflection of sound from these beams became significant when the source was moved close to the array. Finally, the microphones were not sensitive to the lower frequencies that the new technique would allow us to study. All of these factors led to the decision to build a new microphone array that would avoid these problems.

2.2 New Array Design Considerations

When designing the new array system, a set of design goals were decided upon. These are discussed in the following paragraphs.

First, the microphones used in the new array should not be affected by nearby magnetic fields and have a broad, flat frequency response. Inexpensive electret microphones were chosen because they fullfil these requirements.

Second, the suspension system and supporting frame should be designed to securely hold the microphones in position and minimize any sound scattering and reverberation effects. To this end, a sturdy aluminum frame , with rows and columns of thin steel piano wires strung taughtly across it, was designed. Microphones were located at the intersections of the wires.

Third, the new array should be able to record broad band sources. To do this, a set of time samples from the microphones is needed. Consider a square array of N x N elements. The ideal processing method would be to

simultaneously record all of the microphones in the array analogous to taking a photograph since all of the microphones would be recorded at the same instant in time), but this would require N^2 identical processing circuits and would be quite expensive. Today's state-of-the-art electronics allow processing times that approximate simultaneous recordings. Therefore, by processing a single row of N microphones simultaneously (with N identical processing circuits) and then sequentially processing the N different rows at a high rate, we can record the entire array very quickly. Multiplexing the rows with analog switches at the site of each microphone simplifies the wiring of the array and only 2N, rather than N^2, lengths of cable are required. The exposure time of this "acoustic photograph" is determined by the row multiplexing rate. Once the microphones have been multiplexed, analog analysis of the sound field in the time domain is no longer possible. Therefore, digital conversion, storage and analysis is necessary. For state-of-the-art electronics, the data acquisition rate is limited by the analog-to-digital (A/D) conversion time; a typicl value is 1.5usec. For N=16 (a 256 element array) the minimum exposure time of such an acoustic photograph is 16 x 1.5usec = 24usec. This would be quite sufficient for studying sound sources in our frequency range of interest as will be discussed later.

The signal from an electret microphone is typically in the milli-volt region. An A/D converter requires a 10V

signal for proper operation. Therefore, the microphone signal must be amplified. If the amplifier is used after the multiplexing stage, it must be able to respond at the higher multiplexing frequency. A typical operational amplifier can provide 60 dB of gain at the higher multiplexing rate. If a larger gain is needed, it must be provided before multiplexing and should be at the site of the microphone to eliminate any cable noise. A calculation of the total gain needed follows:

Noise level for a typical electret microphone = 0.2uV

Signal to noise ratio for good reconstruction = 30dB[6]

Signal level should be $0.2 \times 10^{30/20} = 6.3$uV

for a signal level of 10V at A/D:

$$\text{Total gain} = 20 \text{ Log}[10/(6.3 \times 10^{-6})] = 124 \text{ dB}$$

Since the gain after multiplexing can be 60 dB, amplifiers at the microphones must provide 64 dB.

The spacing between microphones should be variable to allow different aperture sizes and resolving capabilities. Using N=16 rows and columns, the maximum spacing that will fit in our existing quasi-anechoic chamber is 17.8 cm (7 in). The minimum spacing that allows proper mounting of components in the array is 2.54 cm (1 in).

To determine the temporal sampling rate and highest recordable frequency, we must consider the Nyquist sampling theorem in both space and time. For a microphone spacing of

R, the spatial Nyquist theorem allows a minimum two-dimensional wavelength of 2R to be accurately recorded. Using a microphone spacing of one inch, the highest allowable frequency is f = c/2R = 6.6kHz. If any higher frequencies are present, spatial aliasing will occur. A low pass filter must be used before multiplexing to avoid aliasing in the time domain. The minimum time between microphone samples is 1/2(6600) = 76usec, so the entire 256 element array must be sampled within this time. Thus the obtainable sampling time of 24usec is more than adequate for spatial sampling at 2.54 cm increments.

The digitized data flow and storage of the microphone samples must now be considered. The flow rate is N^2 data words in 76usec. For N = 16, the flow rate is ≈ 3.4 mega-words/sec, too fast for a single input-output (I/O) channel. Therefore, we must use a temporary storage unit that will accept the data at the high I/O rate. Since there are N identical A/D circuits operating in parallel for the multiplexing, let each circuit have its own I/O channel and temporary storage. Then the flow rate becomes N data words in 76usec, or, for N = 16, 200 kilo-words/sec. This flow rate is possible with large scale integrated circuits.

The result of the sampling process will be a time sequence for each microphone in the array. A typical length for a time sequence is 1024 samples. Taking 1024 acoustic photographs with the N x N array would result in a

'filmstrip' of duration T = 1024 x 76usec = ≃ .08 sec for our 6.6kHz source. Frequencies below this allow longer duration filmstrips. The final step in this process would be to read the data (at a suitable rate) from the temporary storage into permanent storage on the computer for processing by reconstruction programs.

2.3 Interim System

Instead of constructing 16 A/D and temporary storage circuits, we found a commercial unit that performed the same operations. It utilizes parallel track-and-hold circuits and a very fast A/D converter with memory. The unit is a LeCroy CAMAC Model 8210 Quad 10-Bit Transient Digitizer that can do four simultaneous A/D conversions at a rate of 1 MHz and store the information in a temporary memory unit. The equipment was ordered, but before it arrived we constructed an interim system that would allow us to continue our nearfield studies of single frequency sound sources. The system was designed to work with the LeCroy unit so that the transition time from the single frequency to the broad band system would be a minimum.

A block diagram of the interim system is shown in Figure 2. It relies on an AR-11 unit in our PDP-11/34 computer to do the A/D conversions of the microphone signals. This unit operates at a rate of 30 kHz. Using the Nyquist theorem, the highest temporal frequency that can be recorded by a 256 element array with a 30 kHz sampling rate is:

$$30{,}000 \frac{\text{A/D}}{\text{sec}} \times \frac{1 \text{ array sweep}}{256 \text{ A/D}} \times \frac{1 \text{ period}}{2 \text{ sweeps}} = 58.59 \frac{\text{periods}}{\text{sec}}$$

$$= 58.59 \text{ Hz}$$

This is much too low to be useful. To study higher frequency sources, we decided to break up the array into smaller groups that we call blocks and take our acoustic photographs one block at a time. Processing fewer microphones at one time raises the maximum temporal frequency that we can record. The result is a time sequence for each microphone in the array. We do not have the capability of studying broad band sources since all of the microphones in the array are not sampled in the 'simultaneous' manner previously described.

Presently, the system is set up to continue our studies of large (typically 30.5 x 61 cm) sources where the wavelength of the radiated sound is typically larger than any dimension of the source. We chose the maximum microphone spacing of 17.8 cm to minimize any finite aperture effects with the large sources. When deciding upon the low pass filter breakpoint, a blocksize of nine microphones (eight array microphones and one reference measurement) was chosen as a standard size. The breakpoint calculation is as follows:

$$30{,}000 \frac{\text{A/D}}{\text{sec}} \times \frac{1 \text{ block meas.}}{9 \text{ A/D}} \times \frac{1 \text{ period}}{2 \text{ block meas.}} = 1667 \text{ Hz}$$

To insure that the filter was active at this value, a

BLOCK DIAGRAM OF SYSTEM

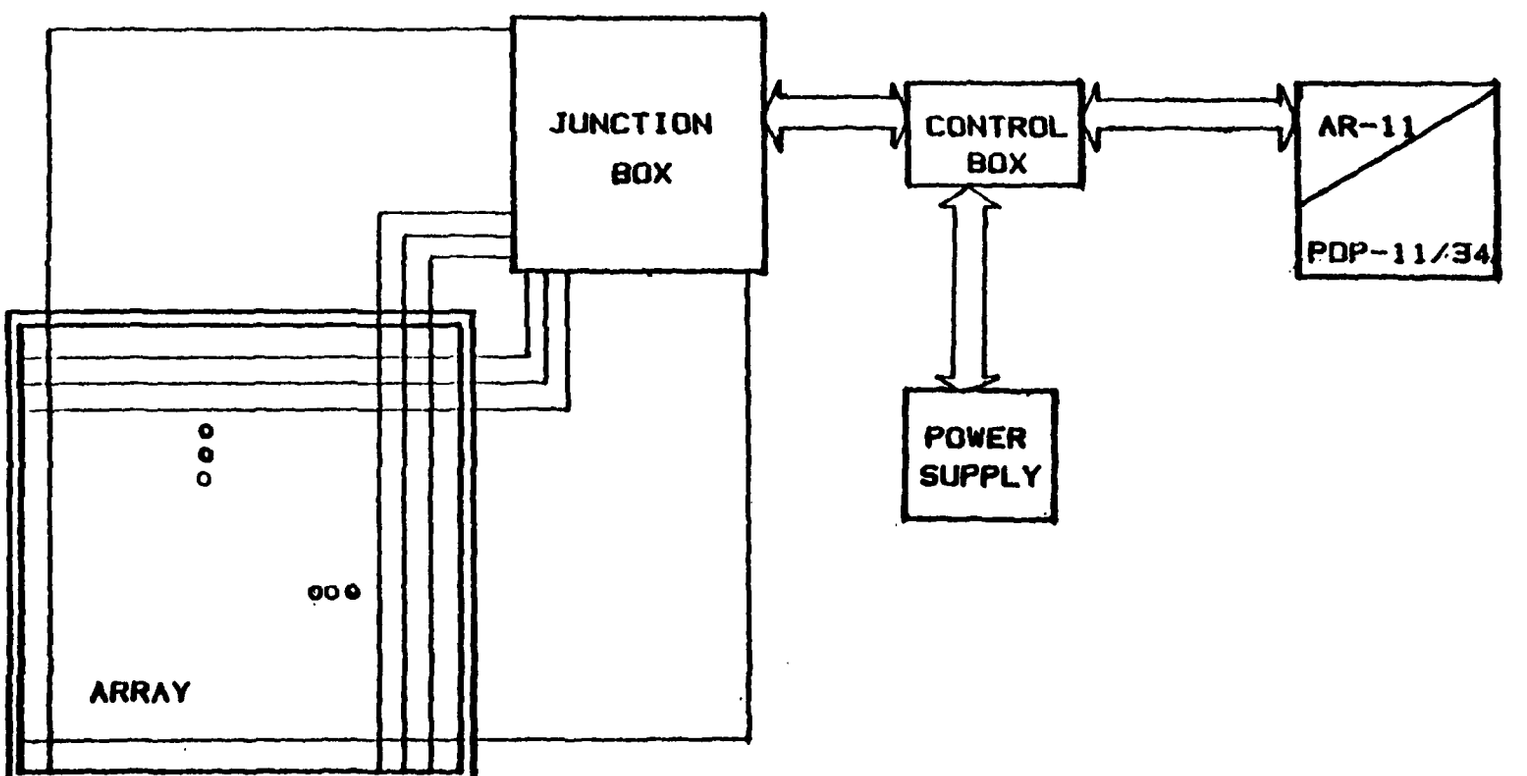

Figure 2. Block Diagram of Interim Data Acquisition System.

breakpoint of 1.5 kHz was selected. The length of the time sequence was chosen to be 128 samples. This is a good compromise between the number of samples required for accurate analysis and the time needed to sample the entire array.

2.4 Details of Construction

2.4.1 Microphone Unit

There were several reasons for selecting a microphone unit rather than a simple microphone. First, the signal voltage from an electret microphone is typically in the milli-volt region. Amplification of this signal is necessary to insure good transmission through the lengths of wire connecting the microphone to the interfacing electronics with a minimum noise pickup. Second, power to the small Field Effect Transistor (FET) in the electret must be supplied. Third, locating the high speed switch at the microphone allows efficient multiplexing and a substantial reduction in the required length of connecting cable as was previously explained.

Figure 3 shows a block diagram of the microphone unit and Figure 4 is the schematic of the circuit used. An explanation of each stage in the block diagram follows.

The electret microphone was chosen because it is small, inexpensive, and has a flat response curve over the frequency range of interest. The size must be small so that

BLOCK DIAGRAM OF MICROPHONE UNIT

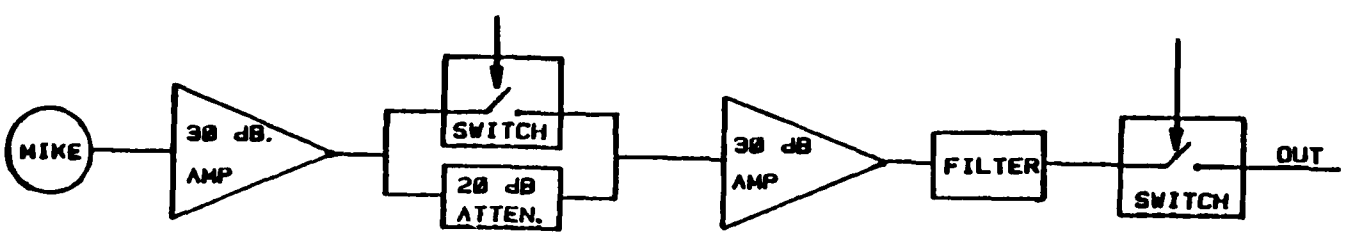

Figure 3. Block Diagram of Microphone Unit

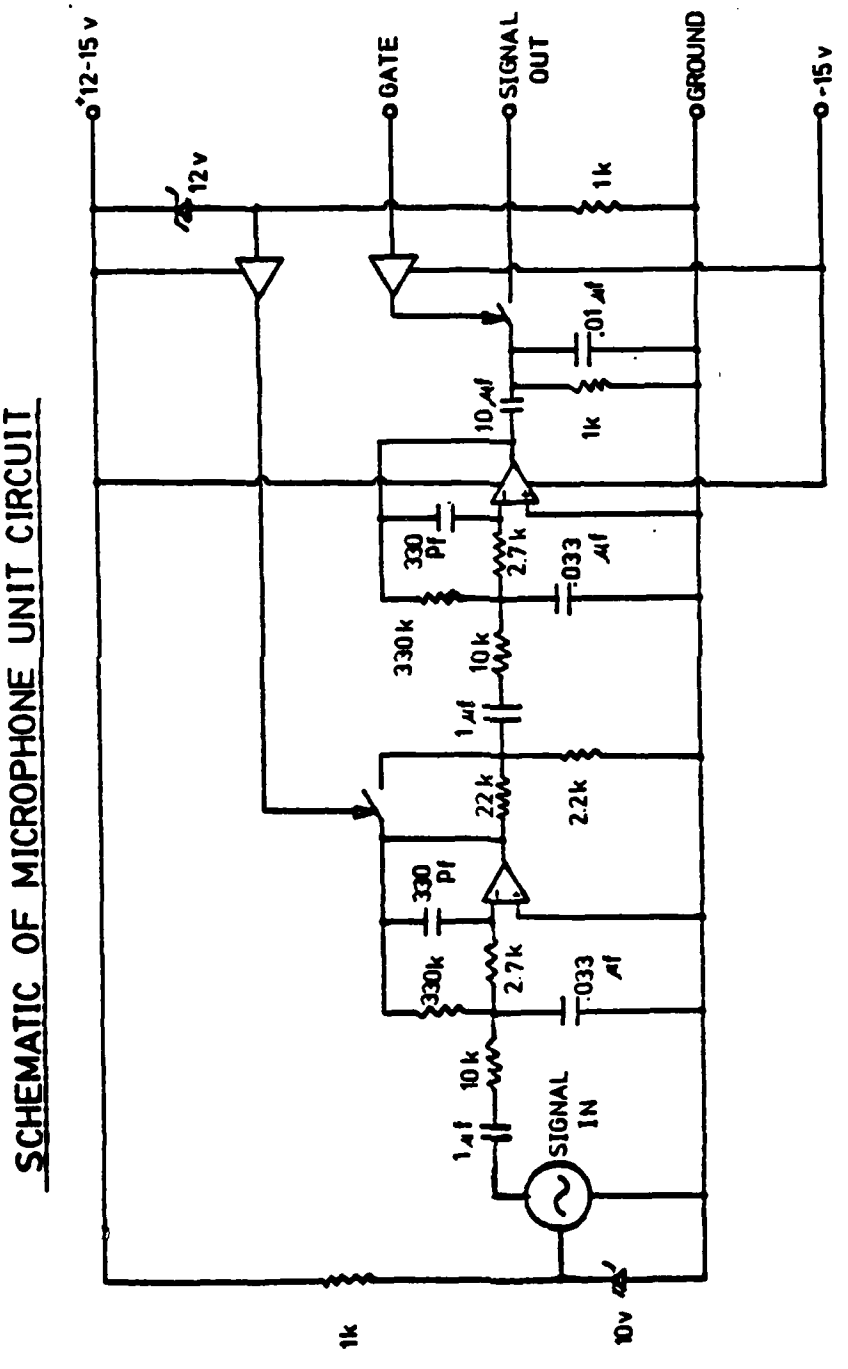

Figure 4. Schematic of Microphone Unit Circuit

the sound field is not disturbed significantly by the microphone. The microphone, a Primo Co. model EM-60B, measures 10 mm dia. x 15 mm high and thus satisfies the small size requirement. The electret microphones were avaliable at a cost of 72 cents each. Since we needed 256 microphones for the array plus some spares, this price was very practical. The frequency range of interest to us is from 100 to 2000 Hz and the response curve for these electrets is flat through this region as well as above and below it. The FET in the microphone requires a +10v supply voltage. Since the positive supply voltage varies between +12 and +15 volts, as will be explained subsequently, a 10v Zener diode is used to maintain the proper supply voltage to the microphone.

The operational amplifier used is a Texas Instruments SN72558 dual amplifier. The circuit chosen provides 30 dB of gain at each stage. In between the two amplifiers is a switchable 20 dB attenuation circuit. This is used if a particularly loud source is being studied that causes the second amplifier to clip. Clipping occurs when the second amplifier reaches a level of 5 volts peak to peak. The schematic shows that this circuit is controlled by an electronic switch. The switch is controlled by the positive supply voltage. A Zener diode holds the gate of the switch at 0 volts when the supply is +12 volts. This corresponds to the switch being in the closed position. When the supply voltage is increased to +15 volts, the gate of the switch is

supplied with +3 volts and the switch opens, activating the attenuator circuit.

A 4-pole filter, 2 poles at each amplification stage, is used to filter out any high frequency components that are not of interest to us. This prevents any aliasing problems when the microphone samples are Fourier transformed. The total filter rolloff is 24 dB/octave. Presently, the breakpoint of the filter is set at 1.5 kHz. Should the need ever arise, the breakpoint may be changed by a plug-in capacitor board on the microphone unit

The high speed switch is a Harris HI-200 SPST CMOS analog unit that contains two switches in one package. One switch controls the attenuator circuit and the other is used to multiplex the microphones. The microphone units in a y direction row all share a common signal out line. The switch is used to turn on one unit at a time along this y row.

The mounting of the components is based on a small printed circuit board with two 14-pin DIP sockets attached to it. This can be seen in Figure 5. A socket is located at the lower end of circuit board. This is where the microphone plugs into the unit. The operational amplifier, filter board, and switch package plug into the female side of the DIP sockets. The top six pins on the male side of the DIP sockets are used to plug the unit into sockets located in the array suspension system. These six pins

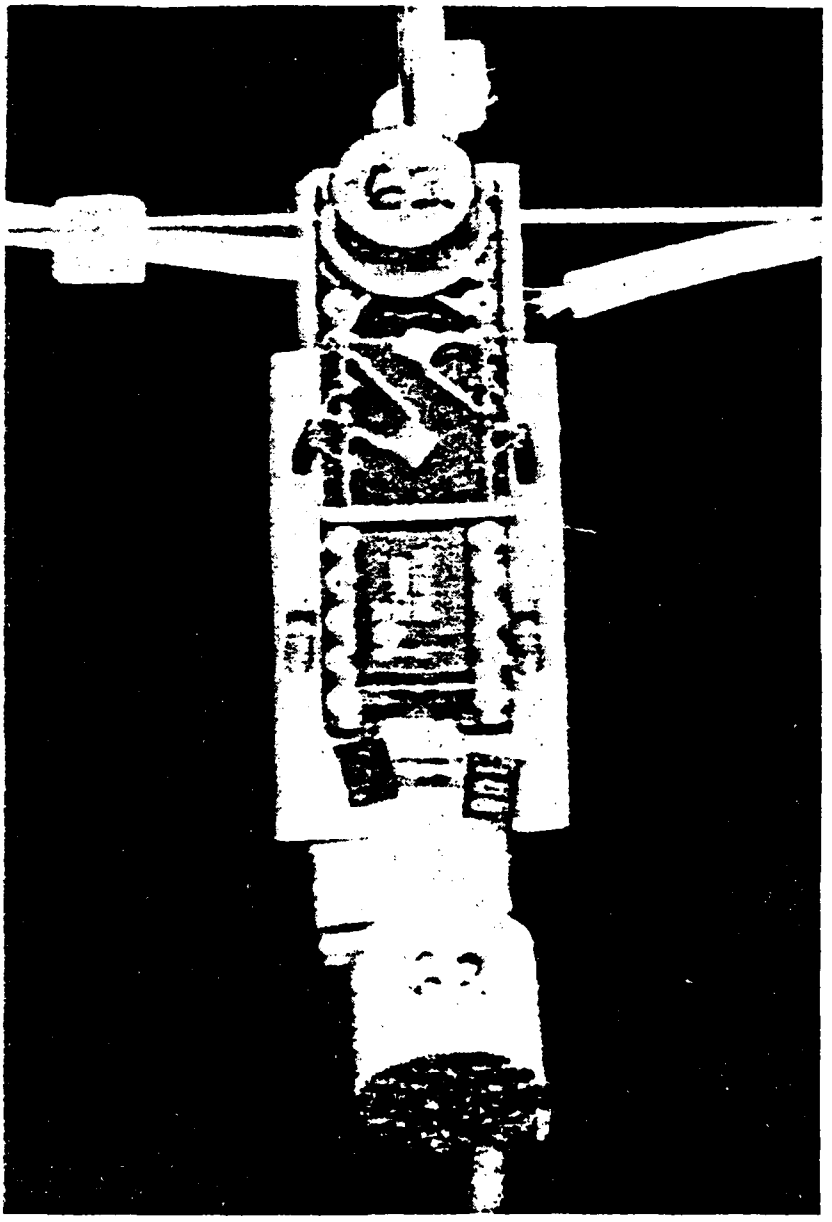

Figure 5. Photograph of Microphone Unit Mounted in Array

serve to hold the unit securely in place and make the necessary electrical connections to the array wiring. If a unit malfunctions, it is easily replaced. All of the major components on the unit itself plug in and are also easily replaced if they fail to operate properly. As with the microphone, the microphone unit must be as small as possible. To this end, all of the components, capacitors, resistors, and diodes, were chosen by their size and were the smallest available at the time of construction. The final measurements of a completed microphone unit are 6 x 1.5 x 1.5 cm.

2.4.2 Microphone Array Support Frame

A drawing of the microphone array support frame can be seen in Figure 6. It is constructed of 10 x 7.5 cm (4 x 3 in) aluminum 'I' beam and measures 3.05 m (10 ft) square, measured internally. Two of the parallel sides split in the middle so that the frame may be folded in half and moved. Two 3.25 m (10 ft 8 in) lengths and four 1.625 m (5 ft 4 in) lengths of 'I' beam were used. The corners were formed by making a 45^0 angle cut at both ends of the long pieces and at one end each of the short pieces. A short length was welded to each end of the two long length pieces. The result was two 'U' shaped pieces. To complete the frame, the two 'U' pieces were joined together to make a square. The split points are held together by a sandwich configuration of two steel plates with the 'I' beam in the

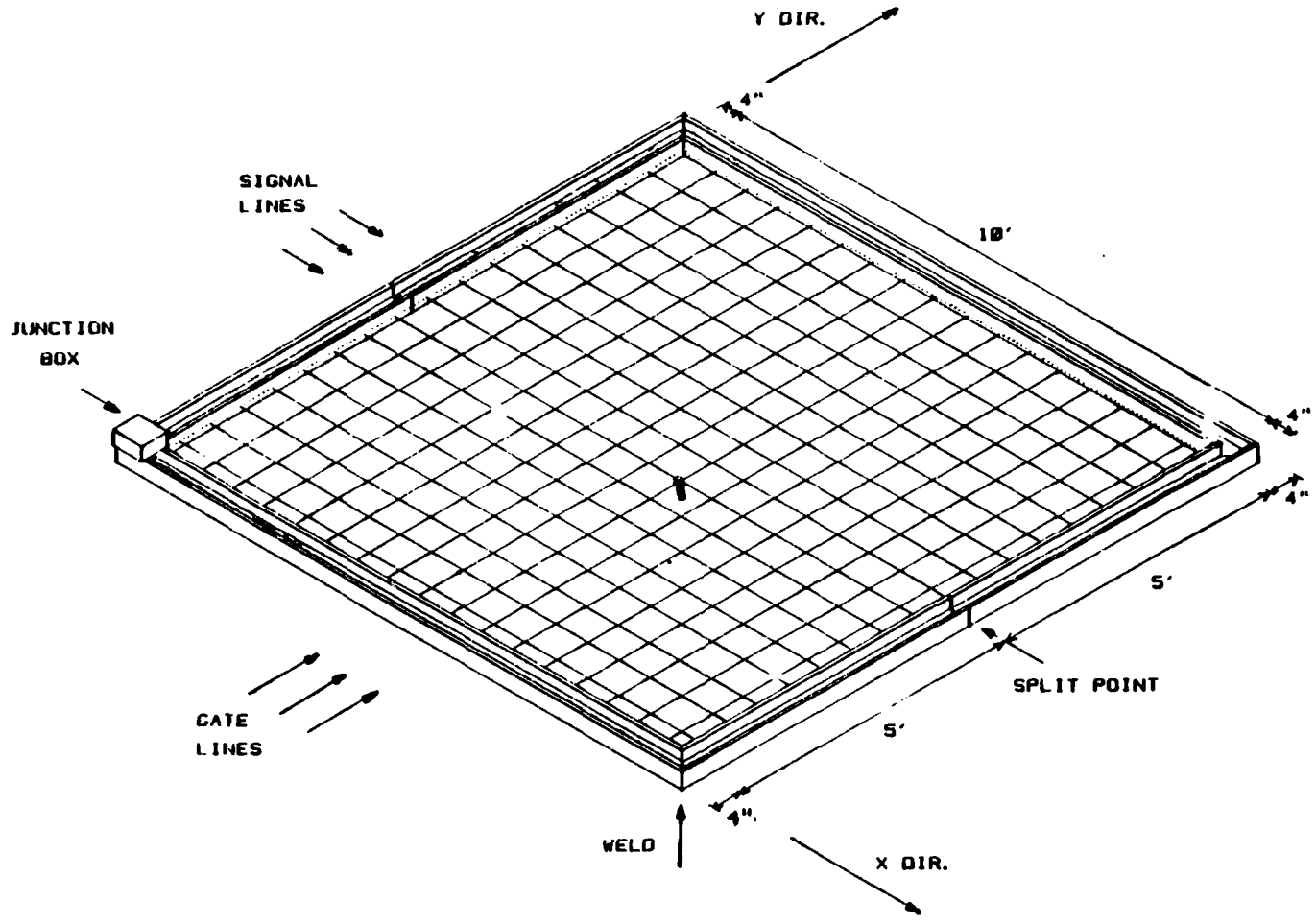

Figure 6. Drawing of Microphone Array Support Frame

middle. The plates are clamped on each side of the split p i t y 5 bolts. This securely joins the two frame pieces. The 'I' beam size was chosen because of its strength and small reflective area. The frame should stay as square as p ssi e when full tension is applied to the piano wires. The worst case deflection of the beam was calculated as follows:

Modulous of Elasticity = E =10.3 x 10^6 lb/in^2

Moment of Inertia = I = 1.31

Load (applied at center of beam) = W = 16 x 30lb = 480lb

Length of Beam = l = 120 in

Max. Deflection at Center = W l^3 / 384 E I

= 0.16 in

A deflection of 0.16 in would not affect the frame shape significantly.

Holes were drilled along the lower inside edge of the 'I' beam on 2.54 cm (1 in) centers. These holes accept tension adjusting bolts that securely hold the piano wires. The spacing between the microphones may be varied from 17.8 cm (7 in) to a minimum of 2.54 cm (1 in) by properly locating the tension adjusting bolts in the holes. This allows adjustment of the array-to-source size. Placing the microphones closer together increases the resolution of the system.

The frame is suspended from the ceiling by a rope and

pulley system attached to each corner of the array. This allows height and leveling adjustment.

The piano wires need to be securely attached to the frame and stretched so that they do not sag in the middle. This was accomplished by designing tension adjustment bolts. The bolts must be long enough to compensate for any elongation in the wire when the wire is stretched. The following is a calculation of the wire elongation due to a 30 lb tension force:

F = Tension Force = 30 lb

L = Wire Length = 120 in

A = Crossectional Area of 0.032 in dia. wire

$= \pi (0.032)^2 / 4 = 8.04 \times 10^{-4}$ in^2

E = Modulus of Elasticity = 30×10^6 lb/in^2

Elongation = FL/AE

= 0.15 in

Thus, the change in length is not appreciable. Two-inch long, 3/8-inch diameter, fully threaded bolts were selected. A small hole that would accept the piano wire was drilled perpendicular to the bolt head. A hole for a set screw that firmly clamps the wire in the bolt head was drilled and tapped. The bolt is placed in the 'I' beam holes and held in place by two locking nuts. For the locking nuts to work properly, they must rest against a parallel face. The inside edge of an 'I' beam is slightly angled, so an adaptor

p ~te was designed that provides a parallel face for the nut to tighten against. It also serves as a mounting platform for a fuse holder and wire terminal. The complete set up can be seen in Figure 7. A worst case calculation of the sag at the middle of the piano wire was made to determine if the suspension system would hold the microphones in a plane:

$$0.11 \text{ lb/mike unit} \times 16 \text{ mike units} = 1.7 \text{ lb}_f$$

$$\text{New Tensile Force in Wire} = \{(30)^2 + (1.7)^2\}^{1/2}$$

$$= 30.05 \text{ lb}_f$$

$$\text{Elongation Change} = 0.15 \text{ in}/30 \text{ lb}_f \times 30.05 \text{ lb}_f$$

$$= 0.15025 \text{ in}$$

$$\text{Length Change} = 0.15025 - 0.15 = 2.5 \times 10^{-4} \text{ in}$$

$$\text{Deflection Down} = \{(60.000125)^2 - (60)^2\}^{1/2}$$

$$= 0.12 \text{ in}$$

A deflection down of 0.12 in (calculated for the worst case of all 16 microphones being placed at the center of the piano wire) is not appreciable and the microphones may be considered to be located across a flat plane.

A microphone unit plug-in socket, an eight pin DIP, is located at each piano wire crossing. Six of the pins are used to support and make electrical connections to the microphone unit. The top two pins were removed. Two small holes were drilled perpendicular to each other at the top of the socket. The piano wires thread through these holes. When the piano wires are tightly stretched, the sockets are oriented in the same direction. This assures proper

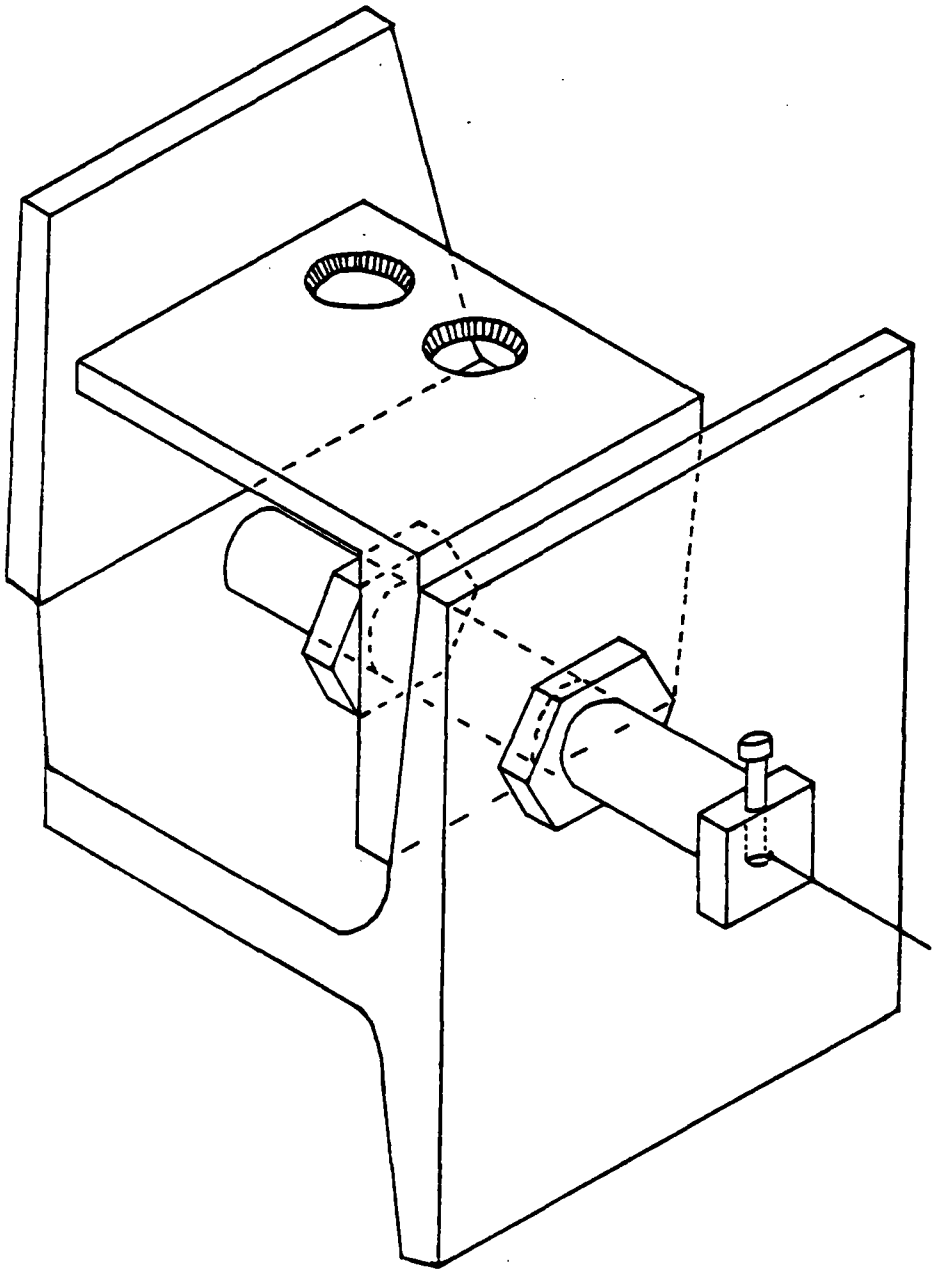

Figure 7. Drawing of Adaptor Plate and Tension Adjustment Bolt Installed on 'I' Beam

alignment and placement of the microphone units when they are plugged in.

2.4.3 Wiring the Array

The wire used to make electrical connections in the array must be as small as possible to reduce any reflective effects. To this end, two-conductor shielded cable with enamel-coated 28-guage wire was chosen. One cable runs along each piano wire, in both directions, making three connections to each socket in that row. The positive supply voltage (+V) and signal out leads run in the y direction and the negative supply voltage (-V) and switch gate voltage run in the x direction. It is important that the gate voltage and the signal out lines do not run in the same cable because of possible cross-talk problems. The shield in both directions is connected to the ground pin of the plug-in socket. At one end of each row, a supply voltage is attached through a protective fuse and the signal out or gate voltage is attached to a mounted terminal. The supply voltages in each direction are bussed together and attached to the junction box. A separate line is run to each signal out and gate voltage row. These are wired to two ELKO multi-pin connectors that plug into a junction box. All cables in the array are secured with wire ties to keep them in order.

2.4.4 Controlling Electronics

Figure 8 is a diagram of the controlling electronics housed in the CONTROL BOX shown in Figure 2. The electronics were designed by Earl Williams. Any one of the 256 microphones may be selected for output by an eight-bit multiplexer, the MIKE POSITION unit in the diagram. As mentioned earlier, the microphones are sampled in groups called blocks. Eight switches located on the CONTROL BOX select the size of the block as indicated by the BLOCK SIZE unit of Figure 8. The BLOCK SIZE number does not change during the sampling process. When the POSITION IN BLOCK counter receives a load signal, the BLOCK SIZE is latched into the counter. The INITIAL MIKE POSTION unit stores the position of the lowest numbered microphone in the block. When the hologram data taking begins, the INITIAL MIKE POSIION is set at zero, which indicates the 'first' microphone in the array. The selected MIKE POSITION is the sum of the INITIAL MIKE POSITION and the POSITION IN BLOCK counter. Note that initially the selected microphone is the sum of the INITIAL MIKE POSITION and the BLOCK SIZE and that the POSITION IN BLOCK counter is a down counter.

At the beginning of the data taking sequence, the microphone multiplexer is disabled and a reference signal measurement is taken. Subsequently, a clock pulse enables the multiplexer and the first microphone is sampled. The next clock pulse triggers the POSITION IN BLOCK counter to

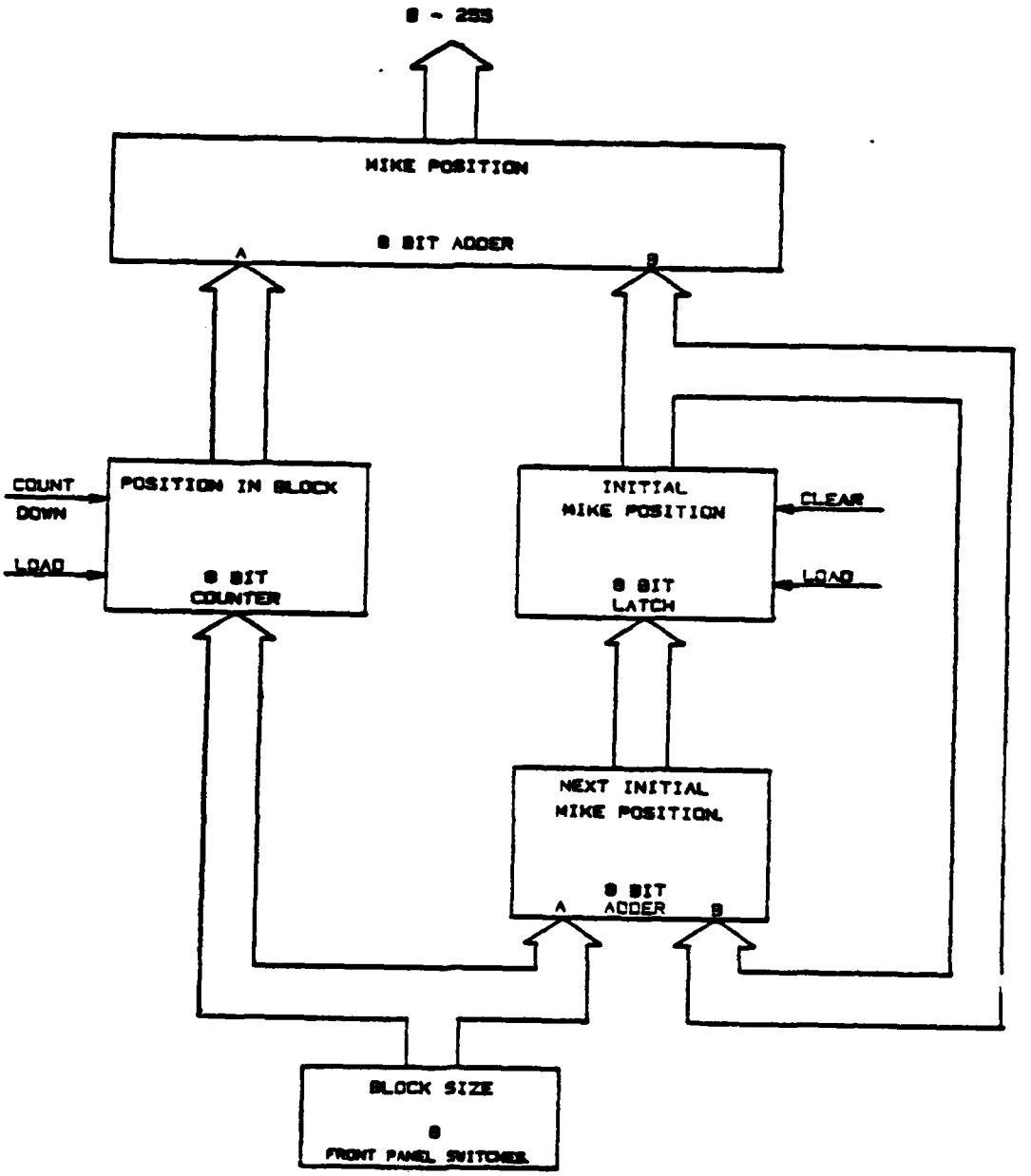

Figure 8. Block Diagram of Data Acquisition Control Electronics

count down by one. This selects the next microphone in the block for output. The countdown process continues until the POSITION IN BLOCK is zero. When zero is reached, the BLOCK SIZE is again latched into the counter and the data taking is repeated. The block is sampled in this manner a selectable number of times to produce a time sequence for each microphone.

When the units discussed above are configured for one particular block of microphones, the INITIAL MIKE POSIION and the BLOCK SIZE are summed to produce the NEXT INITIAL MIKE POSITION. When the first block is finished, the INITIAL MIKE POSITION load is activated and the NEXT INITIAL MIKE POSITION becomes the new INITIAL MIKE POSITION. This gives a new first microphone position, and the POSITION IN BLOCK counter sequences through the new block.

2.4.5 Details of Controlling Electronics Operation

Figure 9 is a detailed drawing of the controlling electronics and Figure 10 shows the circuit used to generate the clock pulses. IC 19, a J-K flip-flop, enables both the count down system and the multiplexer/reference signal output. $\overline{Q}$ starts low. This initiates the following:

1. signals the load on counters IC 6 and IC 8 to latch the BLOCKSIZE from the FRONT PANEL SWITCHES into the counters.

2. combines with a low level from the closed REF/ADR MIKE switch to give a high level from NOR gate IC 16b. This

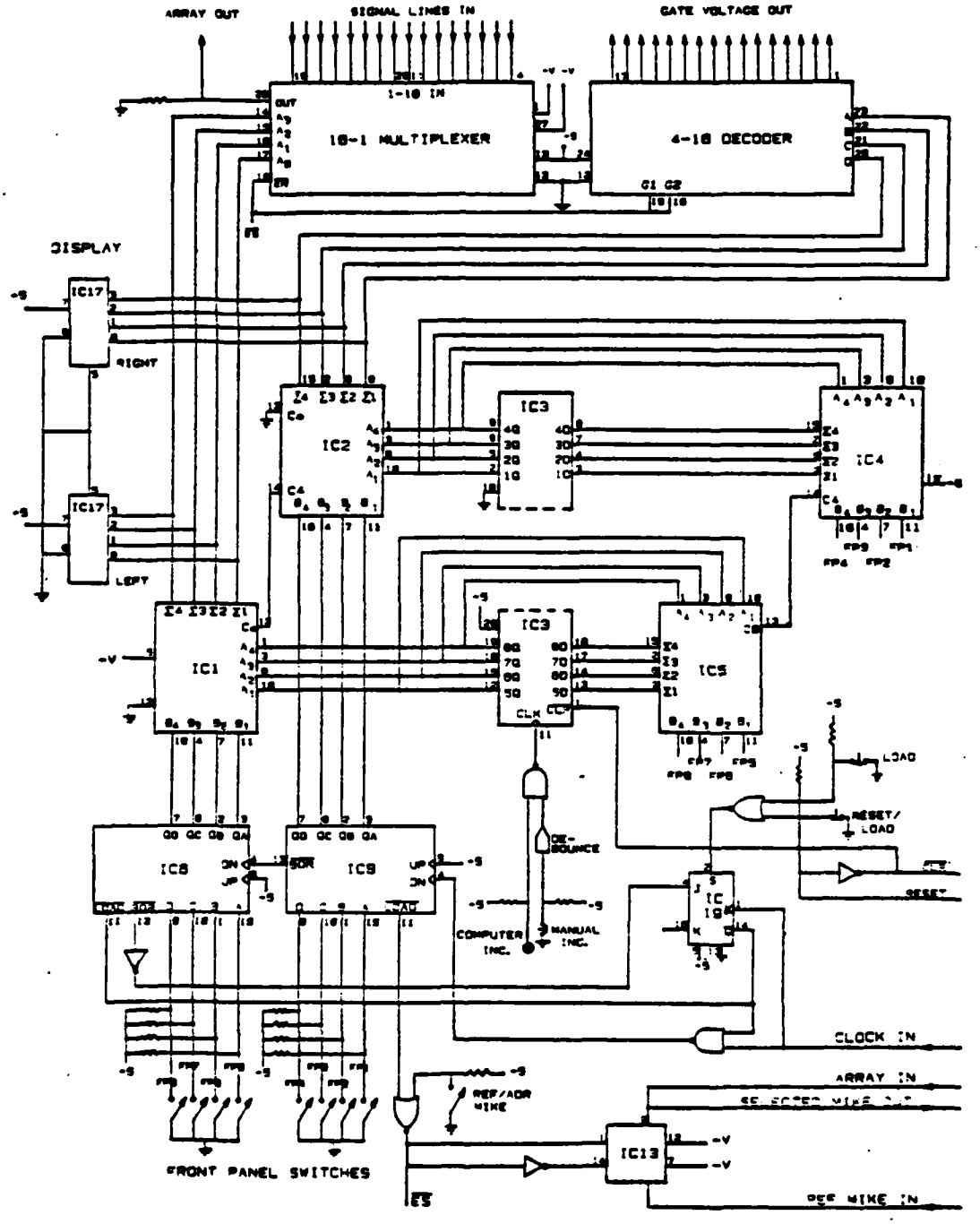

Figure 9. Detailed Drawing of the Data Acquisition Control Electronics Circuitry.

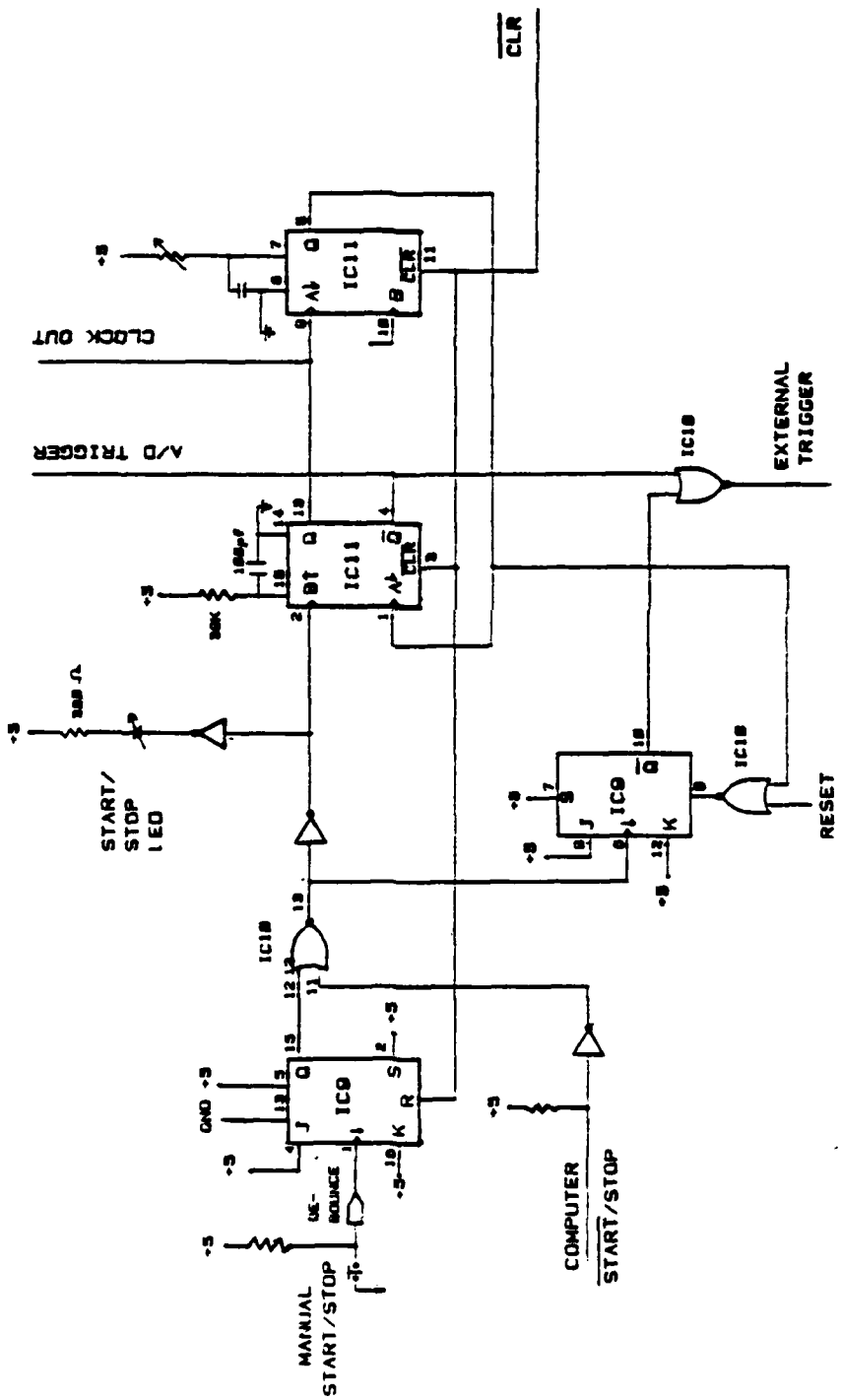

Figure 10. Detailed Drawing of Clock Circuit.

disables the multiplexer output (through $\overline{ES}$) and closes switch IC 13 to place the REF SIGNAL IN on the SELECTED MIKE OUT line.

3. disables the clock from counting down IC 8 through the count-down enable NAND gate IC 15b.

The computer signals the clock to start. The first clock pulse causes the following:

1. signals the computer to A/D convert the signal at its A/D input. This records the reference signal.

2. toggles IC 19 and $\overline{Q}$ goes from low to high enabling the count down through IC 15b. IC 16b enables the multiplexer output and opens switch IC 13, disabling the reference signal.

The microphone selected is determined by adders IC 1 and IC 2. They sum the INITIAL MIKE POSITION from latches IC 3 a and b with the counter outputs from IC 6 and IC 8. IC 1 signals the multiplexer to select one y-row for output. IC 2 signals the decoder to enable a gate line. This selects the first microphone in the block for output. The next clock pulse causes the following:

1. signals the computer to record the microphone signal

2. decrements counter IC 8 by one placing the next microphone in the block on line.

Subsequent clock pulses signal counter IC 8 to count down to zero. After it reaches zero, the next clock pulse sets all outputs high and $\overline{BOR}$ goes low. This signals IC 6 to

count down by one. The last microphone in the block is selected when the outputs from both counters are all low. The next clock pulse records this microphone and counts down IC 8 from all low to all high. $\overline{BOR}$ goes low and IC 6 counts down from all low to all high. The $\overline{BOR}$ on IC 6 goes low, is inverted, and a high level appears at pin J on IC 19 causing $\overline{Q}$ to go low. The first microphone in the block is again latched into the counters while the reference signal is recorded and the cycle repeats, sampling the block a specified number of times.

When the sampling of the first block is completed, the computer stops the clock. Adders IC 4 and IC 5 sum the BLOCK SIZE with the INITIAL MIKE POSITION from latches IC 3 a and b. This is the NEXT INITIAL MIKE POSITION. The computer signals IC 3 to increment the block and the NEXT INITIAL MIKE POSITION is latched to the output of IC 3. The latch output is the A input of adders IC 1 and IC 2 and the new block is ready to be sampled by the counters.

CHAPTER THREE

ACCURACY OF ARRAY

3.1 Purpose

Once the construction of the array was completed and the microphone data were being properly recorded, it was necessary to calibrate the microphones and determine how accurately the system was reconstructing the sound field being generated by a source. We wanted to know the limits of the system and consider possible sources of error. This was broken down into two catagories:

1. Reproducibility - determining the varibility of the reconstructions between successive holograms.

2. Measurement Accuracy - compare a known physical property to one reconstructed by the system to determine how accurately the system represents that quantity.

Velocity was chosen as the physical quantity because the complex velocity at the surface of a source can easily be measured by an accelerometer and directly compared to the complex velocity holographically reconstructed in the source plane. Verifying the velocity rather than the pressure is a more stringent test because the holographic calculation of the velocity is equivalent to taking a numerical derivative of the data which greatly magnifies any variations. If the velocity is correctly reconstructed, then the pressure reconstruction must be at least as precise since the

velocity is obtained from the pressure. Knowing that the reconstructed velocity and pressure are correct insures that the reconstructed intensity is correct since the intensity is the product of the in-phase components of the pressure and the velocity. Therefore, the velocity seems to be a good choice in determining the limits of the system.

3.2 Experimental Technique

The microphone calibration procedure will be reported in detail elsewhere[7], but a brief description is appropriate here. A calibration chamber, similar to a piston phone, was designed and constructed. A reference microphone was used to determine the actual complex pressure in the chamber and all of the microphones were calibrated to this value. The frequency range of the calibration was from 100 to 1500 Hz in 50 Hz increments. This proceedure resulted in all of the microphones being calibrated to within one percent amplitude and one degree phase of each other. The absolute accuracy depended on the accuracy of the reference microphone, which was estimated to be about three percent.

A large, flat rectangular plate measuring 61 x 102 cm was chosen for the velocity experiment because it was a relatively simple source that we had worked with previously. The microphone spacing was 17.8 cm yielding a 4 by 4 square of points on 4.45 cm centers. A grid pattern was drawn on the plate, symmetric about the center, that corresponded to points in the reconstruction. The grid consisted of lines

spaced 4.45 cm. apart: 13 running in the x-direction and 25 running in the y-direction. The measurement points occurred at each x-y crossing giving a total of 325 measurements.

The plate was mounted on the scanning apparatus such that the grid pattern lined up as closely as possible with the microphones. The plate was driven at 248 Hz, a 4,2 mode well below coincidence, and supported by foam strips along its four nodal lines. Two holograms were recorded in succession with care taken to make the measurements as similar as possible. The hologram data were stored in the computer for analysis at a later time.

The plate was then carefully lowered away from the array making sure that the mounting was not disturbed. An ENDEVCO Picomin accelerometer, Model 22, was used to record the surface motion of the plate. An Ithaco Dynatrac 3 Lock-In analyzer was used to determine the amplitude, A, and the phase angle, θ , of the accelerometer signal relative to the plate drive signal. The lock-in output was two DC voltages proportional to $A \sin\theta$ and $A \cos\theta$. The computer recorded these values through its analog-to-digital converter and determined the magnitude and phase of the plate velocity. The entire plate was recorded by placing the accelerometer at each of the 325 grid points.

Once the reconstructed and measured velocities were stored in the computer, they were compared point by point to determine the error between the two velocity files. A

computer program was written to plot histograms of this error in the following way. The program finds the maximum velocity in the reconstruction and sets up 20 velocity bins. Each bin is 1/20 th of the maximum velocity in width. The computer then scans through the reconstruction file and finds all of the velocity values that fall within each bin. For each value in a bin, the error between the reconstructed and measured velocities is calculated. The averaged error of all the velocity values that fall within a bin constitutes the total error for that bin. The error is then plotted as a function of the 20 velocity bins.

An Error Index, a number that would represent the overall error of the histogram, was determined as follows:

$$\text{Error Index} = \frac{\text{SUM}[Ei*Wi*Ni]}{\text{SUM}[Wi*Ni]}$$

where: Ei = the average percent error in bin 'i'
Wi = the weighting factor for bin 'i'
Ni = the number of values in bin 'i'

The weighting factor takes the following form:

$$Wi = \text{number of bins} - i + 1 \; ; \; 1 \leq i \leq 20$$

where 1 = highest velocity bin
20 = lowest velocity bin

Because we expect the higher velocity regions to be more important in the sound field reconstructions, their errors are assigned a higher weighting factor.

To eliminate any offset error, the velocity values were normalized by taking the ratio of the reconstructed to measured values at the center of the plate and multiplying

the measured velocities by this ratio. This greatly improved the file comparison and lowered the Error Index. To determine if this was the best normalization procedure, an iteration technique was used. The normalization was incremented from some starting value in small steps until the lowest Error Index was obtained. This normalization was then used for the histogram plot.

Once the histogram data taking and analysis had been completed, we decided to run a quick check of the array calibration to determine if the system was correctly recording the pressure field. A reference microphone was placed in the array plane. Measurements of the pressure over a point on a source were recorded by the reference and an array microphone. The errors between these measurements were compared at different frequencies and were found to be inconsistent. We found that the discrete Fourier transform (DFT) was returning a pressure amplitude that was always lower than the reference amplitude. This error was caused by the fact that the source was being driven at a frequency F_o that did not correspond to any of the discrete frequencies (multiples of $2\pi/Ndt$, where the quantities N and dt are described below) set up by the DFT. It is easy to show that to correct this problem, one must multiply the amplitudes returned by the DFT by a correction factor of the form:

$$\text{Correction Factor} = \frac{\text{SIN } (x)}{(x)}$$

where $x = \pi * N * dt * (F_n - F_o)$

N = number of samples
dt = sample time
F_n = nearest DFT bin frequency to source frequency
F_o = source frequency

This factor was not originally included in the programs because we were not interested in the absolute accuracy of the system at that time. Incorporating this correction factor into the data taking programs solved the varying error problem, resulted in a typical error between reference and system measurements of about four percent or 0.3 dB, and improved the absolute accuracy of the system. The relative accuracy remained the same.

3.3 Results

The reproducibility of the system was determined by taking two successive holograms and using the histogram program described earlier to compare them. The Error Index from this histogram, seen in Fig.11, shows that the system is typically reproducible to within seven percent or about 0.59 dB.

A histogram used to determine the measurement accuracy can be seen in Fig.12. The Error Index for this histogram shows that the system error is typically within eighteen percent or 1.4 dB. This would seem to indicate that the system is correctly representing the velocity over the

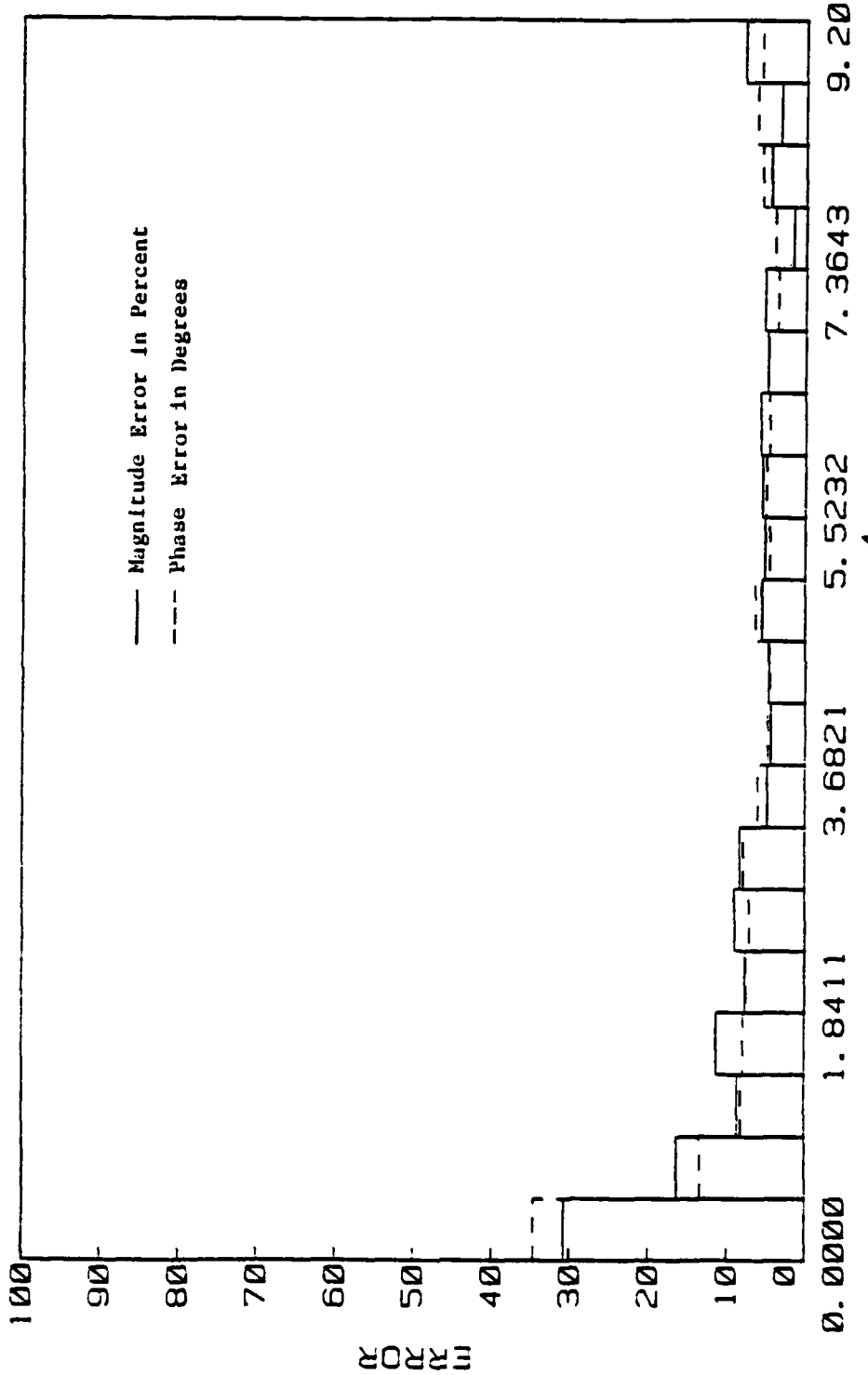

Figure 11. Velocity Amplitude Histogram Showing System Reproducibility

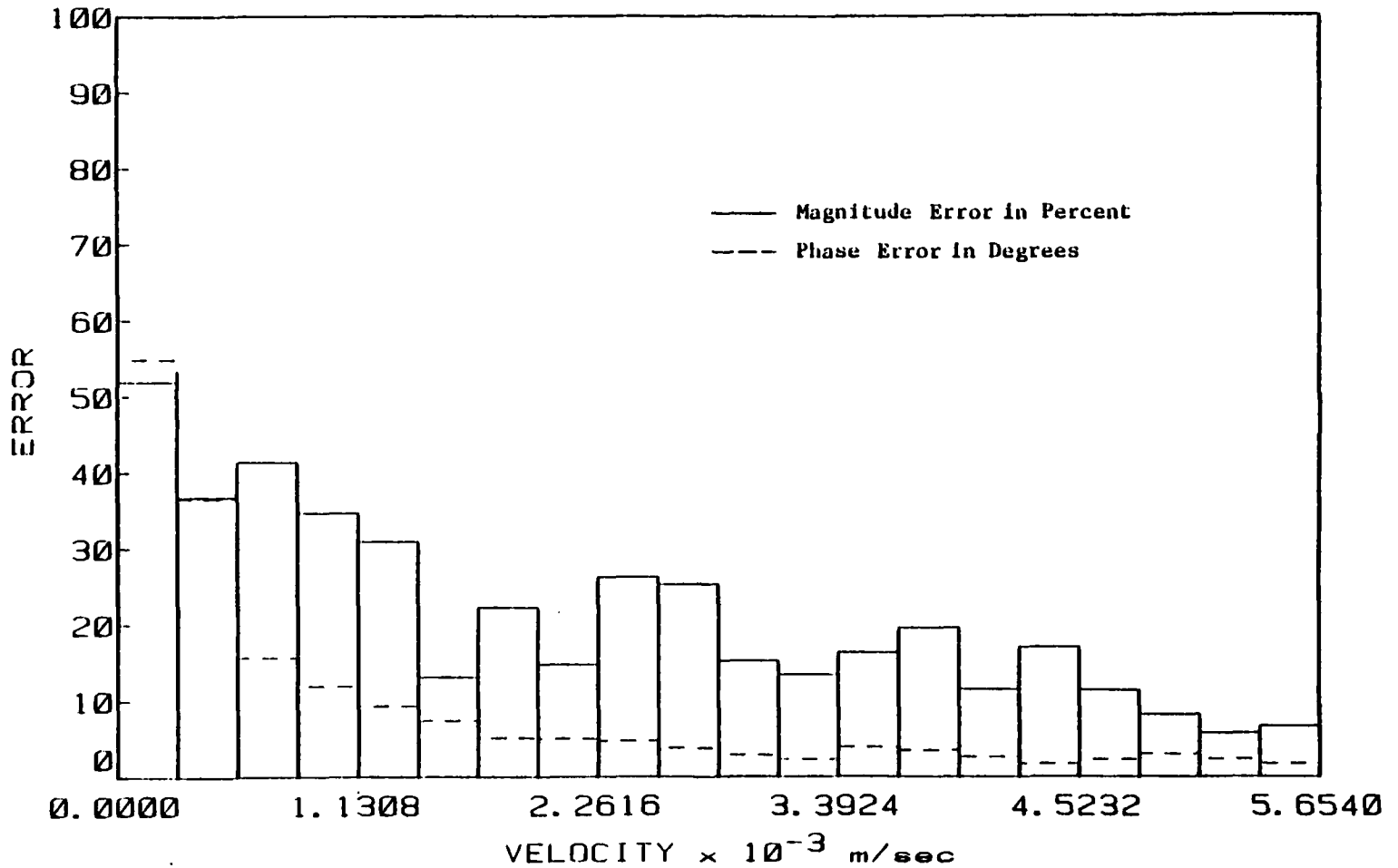

Figure 12. Velocity Amplitude Histogram Showing Measurement Accuracy

surface of the source, but some of the absolute values of the velocity differ from those measured by the accelerometer. The phase differences between the hologram and measured data are typically less than 5 degrees.

Other possible sources of error that time did not allow me to study are as follows:

1. The standing wave pattern set up within the measurement space changes when the source is moved beneath the array to fill in points betwen the actual microphone spacings. Changing the standing wave pattern may change the pressure recorded by the microphones and therefore introduce an error into the data. The effects of changing the standing wave pattern would be quite difficult to determine, but the problem may be eliminated by keeping the source stationary and moving the array to fill in points. Standing waves could still exist within the space, but the pattern would not change appreciably if the array was moved. To do this, a system for moving the array would have to be designed and constructed.

2. The hologram data are smoothed during the reconstruction process to make the reconstruction less noisy. The smoothing process changes the amplitude and phase of the data slightly, but is necessary for clear, analyzable, reconstructions. This must also be a source of error and requires a detailed study to fully

understand its effects.

3. The microphones in the array are not all exactly on 17.8 cm centers. This was realized after these experiments were completed. Some microphones may be as much as one-half inch offset from their neighbor. The result of this error is that hologram points may not be lining up exactly with accelerometer data points on the plate.

4. The positioning system may not be moving the source orthogonally to the array, again resulting in the hologram points not lining up with accelerometer data points. If the array was moved instead of the source, this source of error would no longer exist.

CHAPTER FOUR

EXAMPLE OF TECHNIQUE USING A RELATIVELY SIMPLE SOURCE

4.1 Introduction

The rectangular plate used for the verification experiments discussed in Chapter 3 nicely demonstrates the technique in actual usage. The center driven plate is a relatively simple source in that there are no ribs or discontinuities across it and its modal patterns are well known. Therefore, we can predict what the reconstructed characteristics should be and compare them with the actual reconstructions.

When setting up the experiment for Chapter 3, a mounting for the plate had to be selected. This required that the plate be supported in the same manner throughout the repeated application and removal of the accelerometer. The easiest mounting scheme that would fulfill this requirement was to place the plate on a one-inch-thick sheet of foam. This would uniformly support the plate and not allow it to move during the experiment. To isolate the foam from the scanning apparatus, two two-inch-thick sheets of fiberglass were placed between them. Both the foam and the fiberglass were cut to the dimensions of the plate. Reconstructions of this configuration showed that there was a significant velocity developed in the air just outside the boundaries of the plate, which was probably caused by diffractive effects.

The data smoothing process tends to average the velocities recorded at the plate edge with the velocities recorded in the air just outside the edge. Since the air velocity is usually 180 degrees out of phase with the plate edge, this effect would pull down the velocity amplitude measured at the edge. It should be noted that this averaging would happen even in the theoretical limit of zero velocity outside the plate boundaries. We wanted to minimize this effect and decided to try a different mounting.

Knowing that the plate was being driven in a (4,2) mode, we decided to remove the foam sheet and replace it with foam strips located along the four nodal lines across the short dimension of the plate. This configuration supported the plate correctly and we hoped that this would reduce the diffractive effects. Reconstructions showed that the velocity outside the plate had diminished but was still present.

Next, we thought that the large reflecting area of the fiberglass sheet directly below the plate might be contributing to the diffractive effects. We decided to remove these sheets and replace them with support strips consisting of 4 x 4 inch blocks of fiberglass extending along the short plate dimension. The foam strips used before were placed on top of the fiberglass and were again located along the nodal lines. This configuration supported the plate correctly and further decreased the diffractive

effects. It was therefore selected as a satisfactory mounting. Previous work with the plate point-supported indicated that the diffractive effects were less, but the point-supported plate would not have been stable enough for the accelerometer measurements.

4.2 Results

Figure 13 shows an overhead view of the plate velocity with the full fiberglass/foam sheet mounting. The symbols in the legend represent levels that are within 5, 10, 15, and 20 dB less than the maximum level recorded on the plate. The positive (POS) and negative (NEG) symbol sets refer to areas of vibration that have a phase difference of 180 degrees in the velocity reconstructions or to areas of positive and negative intensity in the intensity reconstructions. By comparing this figure with Figure 14 (which shows the plate velocity with support strip mounting), one can see that aside from a lessening of the diffractive effects, the nodal structure and velocity amplitude are quite similar. However, when comparing the intensities of these two support cases, an interesting effect is observed. The intensity reconstruction of the foam mounted plate is shown in Figure 15. Note the large positive intensity region at the center of the plate where the driver is located. Figure 16 shows the intensity reconstruction for the strip supported plate. Comparing these two reconstructions reveals a large change in the

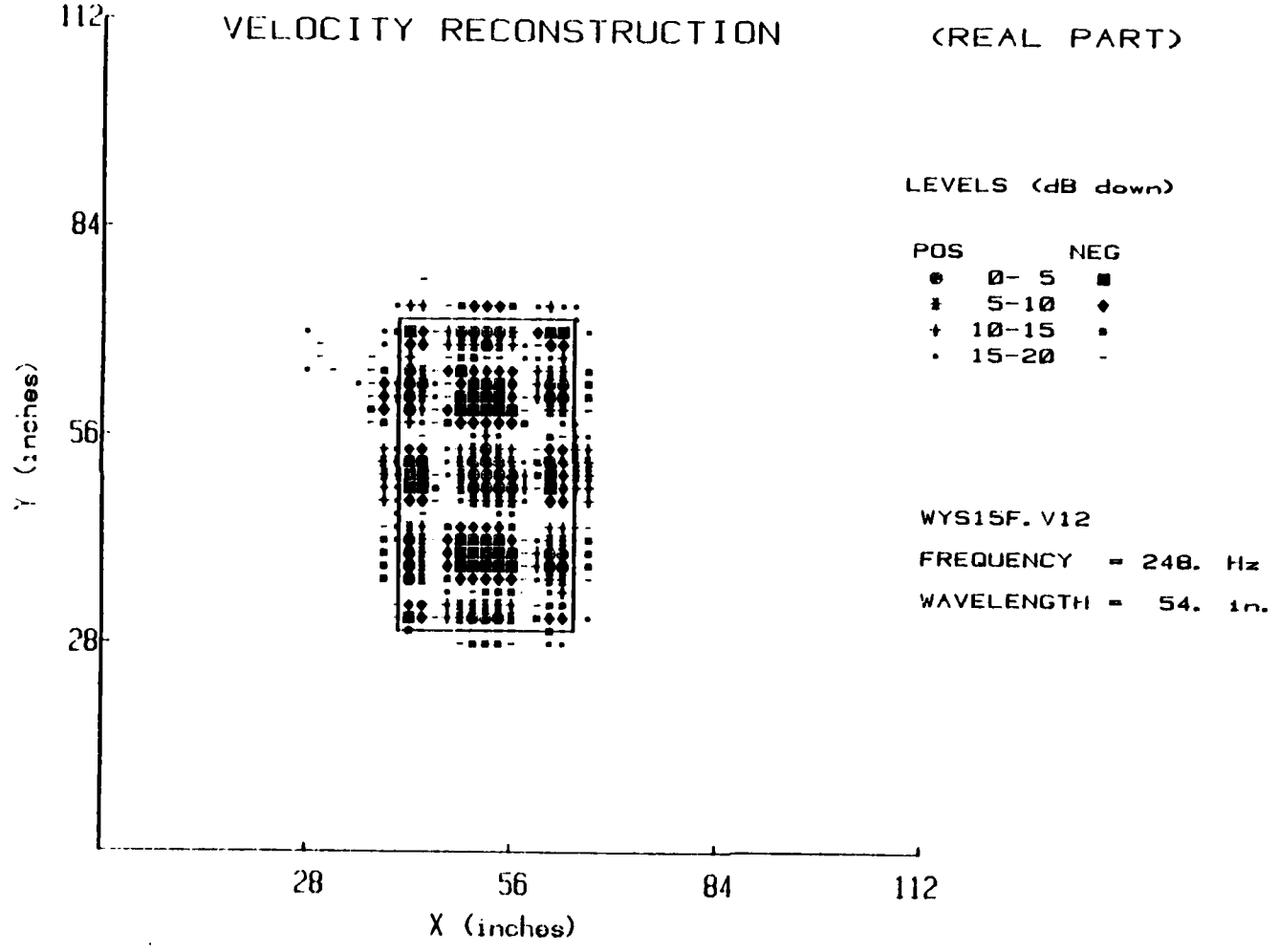

Figure 13. Velocity Reconstruction of Plate with Fiberglass/Foam Sheet Mounting. Note Nodal Structure of the (4,2) Mode.

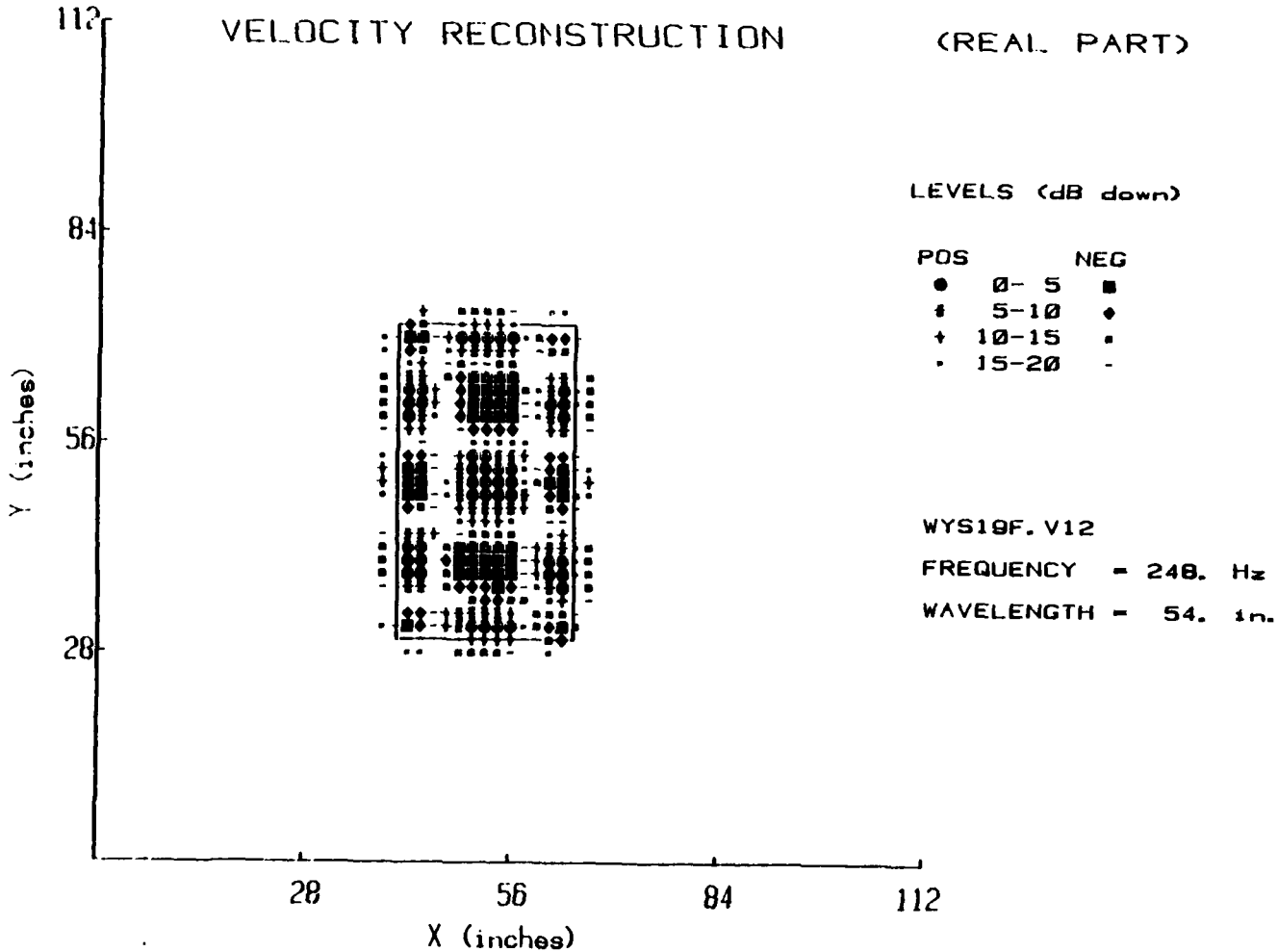

Figure 14. Velocity Reconstruction of Strip Supported Plate. Note Similar Nodal Structure but Less Diffraction Than Fig. 13.

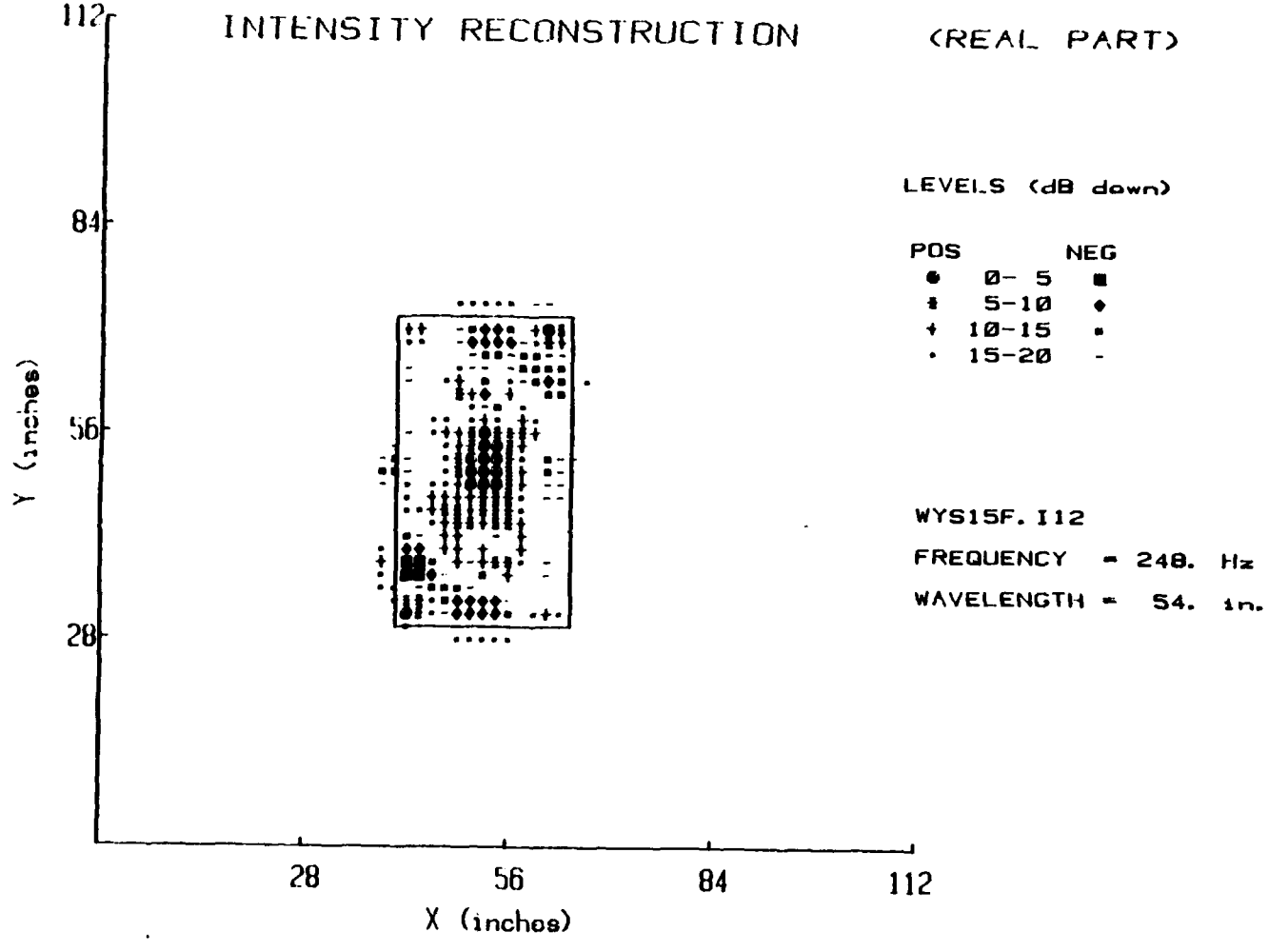

Figure 15. Intensity Reconstruction of the Fiberglass/Foam Sheet Mounted Plate

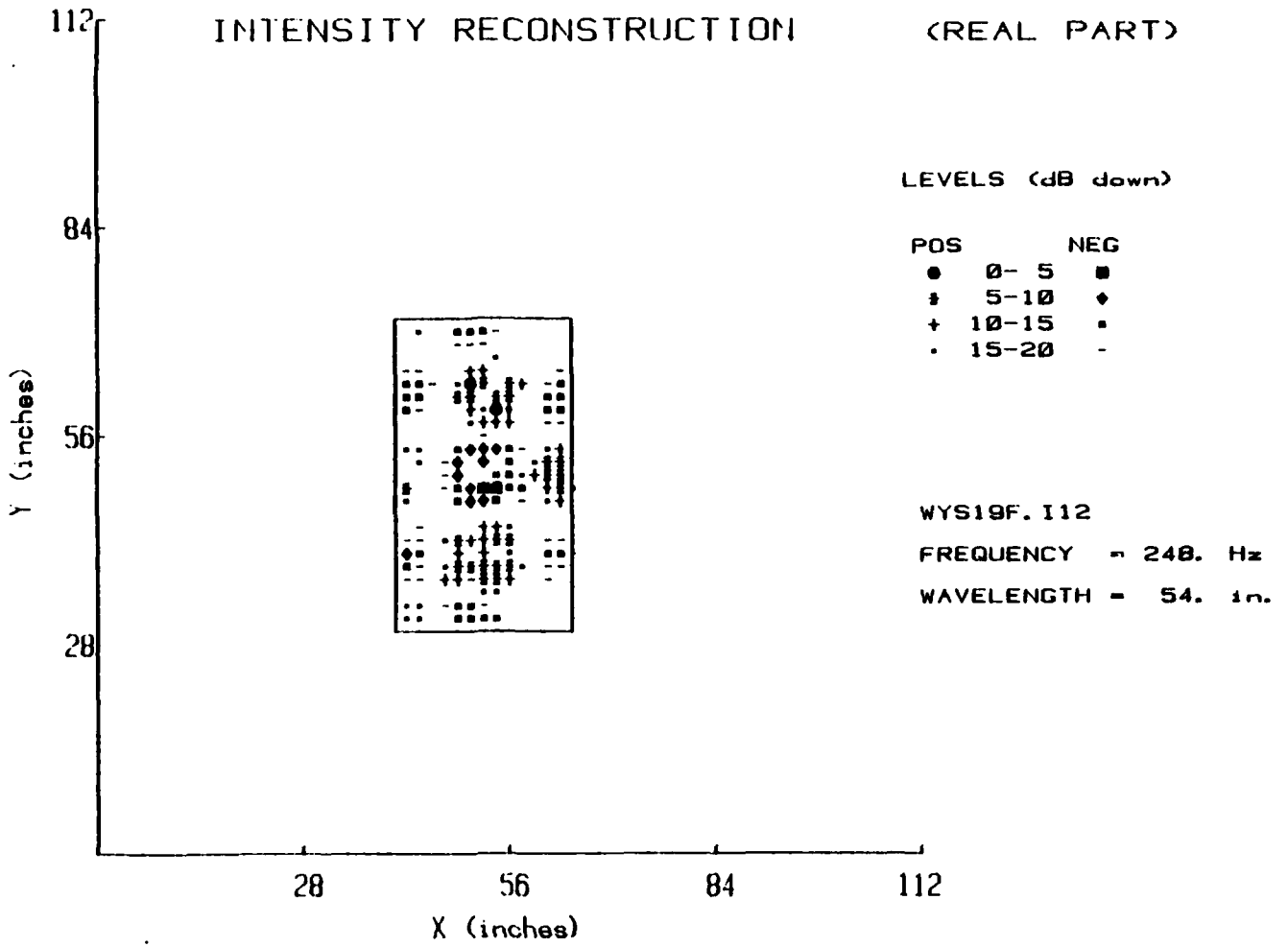

Figure 16. Intensity Reconstruction of Strip Supported Plate.

intensity. The strip supported plate shows a large negative intensity region near the driver with neighboring areas of positive intensity. A discussion of this effect follows:

The real part of the intensity is defined as one-half the product of the in-phase components of the pressure and the velocity. i.e.;

$$I = 1/2\ p\ v \cos(\theta)$$

where θ = the difference in phase angles between the pressure and the velocity

Analysis of the foam-supported plate data reveals that θ near the center of the plate is typically -68 degrees. The cosine of -68 is positive and therefore a positive intensity is observed. The strip supported plate shows a typical θ of -98 around the center with neighboring areas having a θ of about -81. This small change in θ results in a large intensity change. A similar change in θ for the foam supported plate would not result in as great an intensity change. Since θ for the strip-supported plate is close to -90, the sound field is quite reactive. This almost totally reactive sound field does not produce much radiated energy and is therefore a poor radiator of sound. The sound field around the foam supported plate is much less reactive, making it a better radiator of sound even though the plate is subjected to much more damping. This may be explained by considering the radiation from an infinite plate that is point driven. The flexural waves produced by the driver

propagate away from the driven area through the plate. Since the plate is infinite, these flexural waves are not reflected. In this case, the driven area produces the radiated energy[8]. In our case, the foam supporting the finite plate can be expected to absorb some of this energy. If enough of the flexural wave's energy is absorbed by the foam, the damped plate begins to act as the infinite plate and most of the radiated energy is produced at the driver.

On the other hand, once most of this damping is removed by strip-supporting the plate, the flexural wave's energy is not as highly attenuated and more of this energy may be reflected from the plate's boundaries. This results in a more reactive field near the plate and less radiated energy is produced. There are still some losses present and some sound energy is radiated as can be seen in Figure 17. This figure nicely shows the non-radiating, circulating energy flow present in the strip-supported plate.

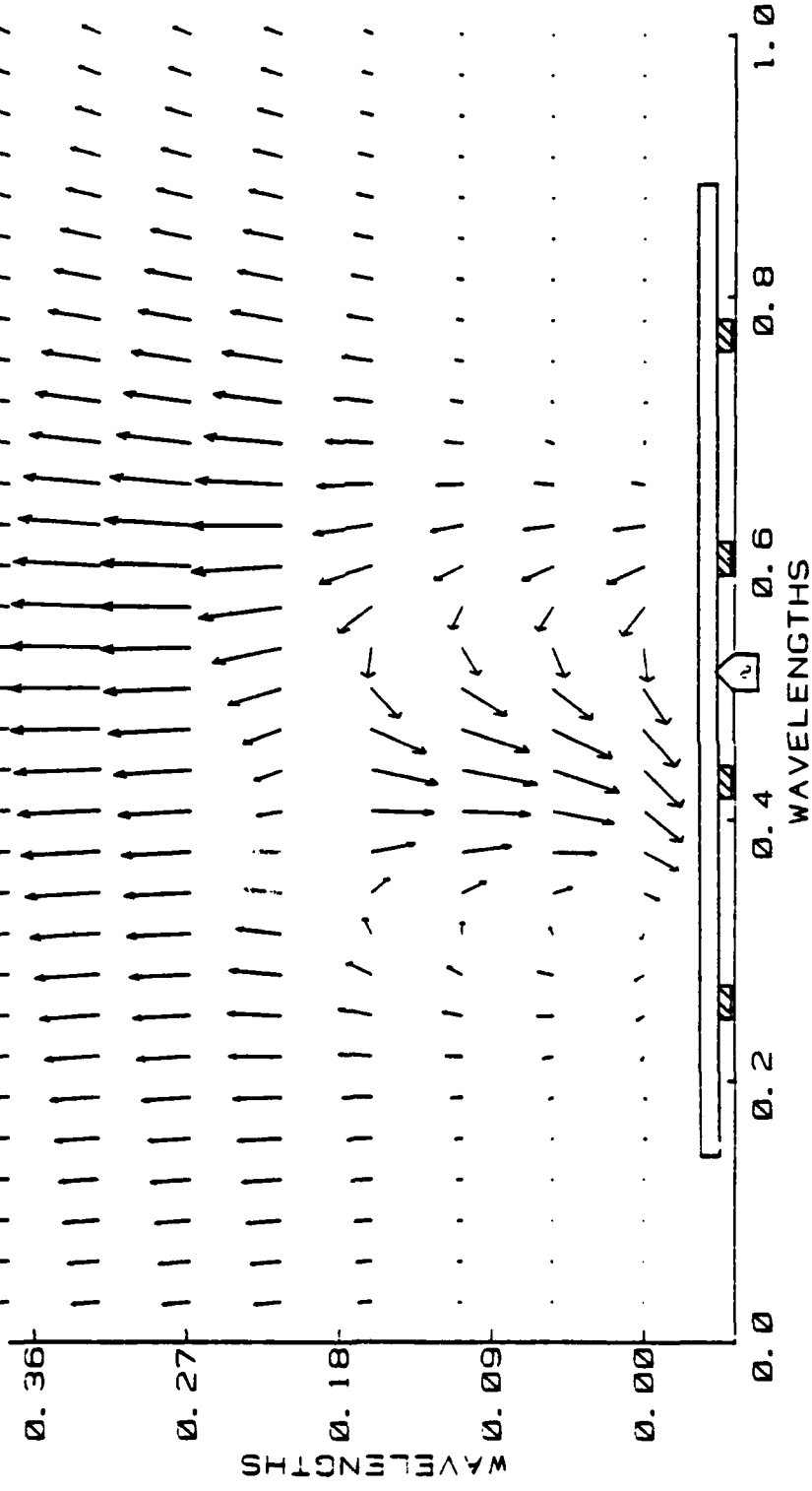

Figure 17. Energy Flow Map of Strip Supported Plate, Side View Along the Long Dimension of the Plate. Note Circulating Flow that Is Unmeasurable as Little as a Quarter Wavelength From the Plate.

CHAPTER FIVE

EXAMPLE OF TECHNIQUE USING A COMPLEX SOURCE

5.1 Introduction

In the previous chapter, results of a plate source with different mountings were presented. The technique was able to detect changes in the intensity due to different mountings where there seemed to be no corresponding change in the velocity. The next and final step in this work was to use the technique to study a complex radiator. To qualify as being complex, a vibrator may have a non-trivial shape or inhomogeneous composition, and an exact mathematical solution for its sound-generating properties does not exist. To enhance the relevance of this research, it would be helpful if the source had some general academic interest. To this end, we chose a string-excited enclosed cavity with radiating port, better known as a guitar, to be the complex source.

The guitar is indeed a complex vibrator. Its shape is not readily adaptable to any coordinate system and the internal ribbing makes the plates inhomogeneous. The source has been of interest in the past[9, 10, 11], and our technique seems ideally suited to study it since we can reconstruct many important properties of the source with one measurement. Previous work gives us an idea of what to expect from the plate velocity, but to the author's

knowledge there have never been any studies undertaken to experimentally determine the acoustic energy produced and radiated by the guitar.

5.2 Experimental Technique

A Martin steel-stringed acoustic guitar was chosen for the experiments. Unlike many other experiments, the guitar was totally intact and tuned to concert pitch. The guitar was point supported at three locations: the neck and two points on the backside edge of the lower bout (The guitar body is referred to as the bout. The lower bout is the area below the rose, or sound hole, and the upper bout is the area above the rose. In this discussion, the bout will refer to the top of the guitar unless otherwise noted). In an effort to excite the instrument as closely as possible to actual playing conditions, the steel strings were used to drive the instrument. A small electro-magnet was placed near the string to be excited. An AC current was passed through the electro-magnet at the frequency necessary to oscillate the string at resonance. An electro-mechanical shaker placed on the bridge of the guitar would excite plate modes more dramatically than the driven string, but we were interested in examining the guitar as it would be played.

The actual study was divided into two parts. The goal of the first study was to locate modes of the guitar top plate and compare various results obtained with our technique to those obtained with other techniques (holographic

interferometery in particular). The second study focussed on the behavior of the guitar in between these so called natural modes. By obtaining reconstructions of the top plate over the first two octaves of the instrument's frequency range, we hoped to see changes in the top plate velocity and radiation characteristics. This information has not previously been available and should be of interest.

5.3 Results

5.3.1 First Study

At first, we wanted to be able to reproduce some of the results found in the literature. There appear to be several accepted modes of vibration for the top plate of the guitar. These can be seen in Figure 18. The first plate mode appears as a breathing mode where the entire lower bout is vibrating in phase. The second plate mode appears as a dipole mode where the lower bout breaks up into two areas vibrating 180^0 out of phase. I was able to locate both modes in the experimental guitar but will concentrate on the dipole mode in this discussion. The frequency of the dipole mode was determined by placing a shaker on the bridge and two accelerometers near points on the plate that could be expected to be vibrating 180^0 out of phase. Once the frequency of the dipole mode had been determined, a string was tuned to that frequency and excited by the electromagnet. Velocity reconstructions at this frequency reveal the strong dipole mode in the lower bout, but other effects

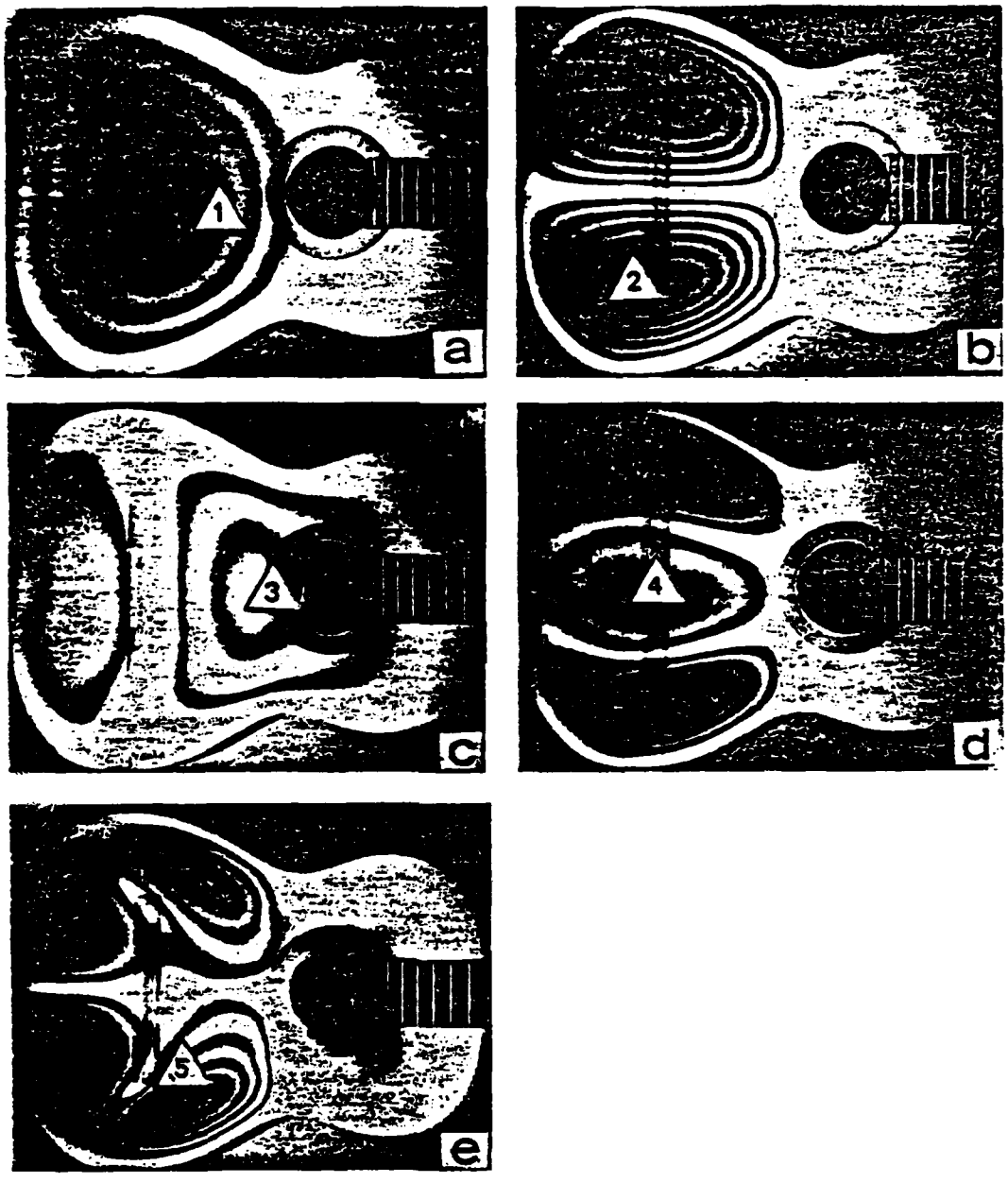

Figure 18. Holographic Interferograms of Guitar Top Plate Motion. (a) 185 Hz, (b) 287 Hz, (c) 460 Hz, (d) 508 Hz, (e) 645 Hz. (Source: Jansson, Acustica 25, 98 (1971))

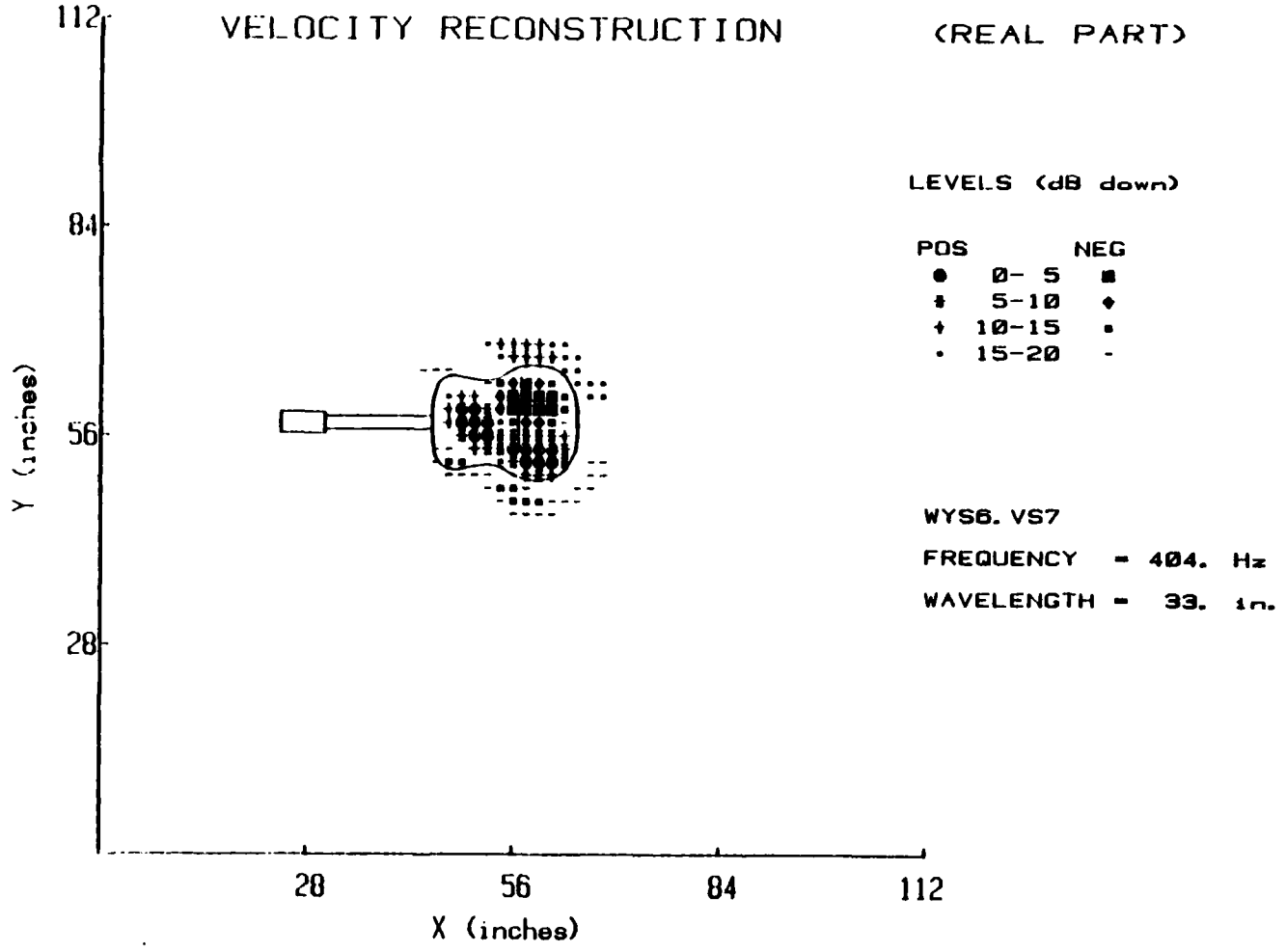

Figure 19. Velocity Reconstruction of Guitar in Lower Bout Dipole Mode. Note That the Greatest Activity Takes Place at the Rose.

are present as can be seen in Figure 19 (The symbols in the legend represent levels that are within 5, 10, 15, and 20 dB less than the maximum recorded on the top plate. The positive (POS) and negative (NEG) symbol sets refer to areas of vibration that have a phase difference of 180 degrees in the velocity reconstructions or to areas of positive and negative intensity in the intensity reconstructions). Here the motion of the air in the rose is evident as well as some diffractive effects outside the boundaries of the guitar. These diffractive effects are probably due to the motion of the back plate of the guitar. It is important to note that the interferometry technique used to create the pictures in Figure 18 cannot represent the motion of the air in the rose or outside the guitar boundaries. A dipole source is generally accepted to be a poor radiator of sound. Using the results obtained from interferometry, one might be led to conclude that the guitar does not radiate well at this frequency. However, our reconstructions show an area of large velocity located at the rose. The intensity reconstruction shown in Figure 20 indicates that the rose is a substantial energy-producing area. The energy flow map of Figure 21 clearly shows that the rose is the major contributor to the radiated sound field. Figure 22 shows the nearfield short-circuit that occurs due to the circulating energy flow at t wer bout of the guitar. This results in little radiated energy originating at the lower bout. Being able to record the motion of the air in

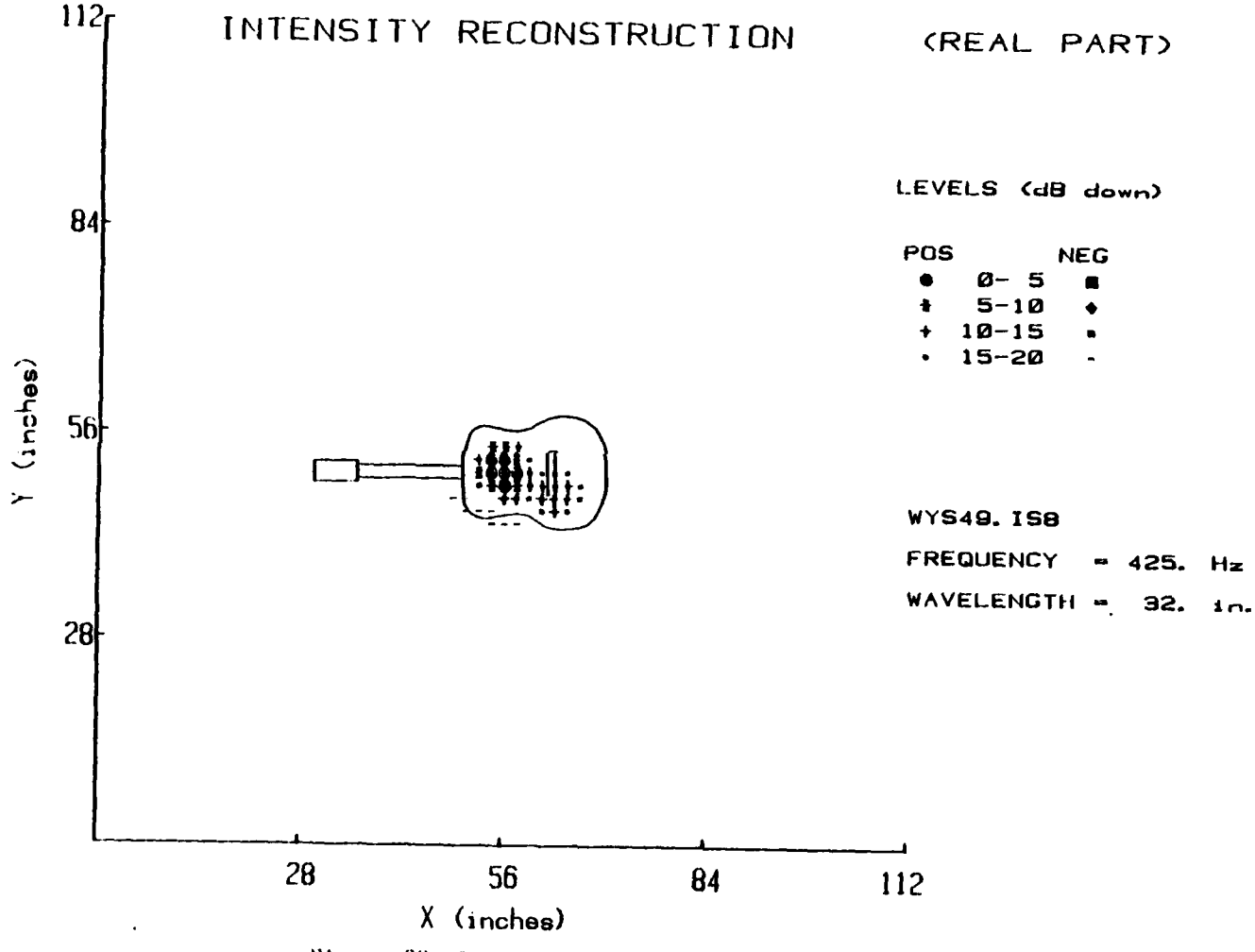

Figure 20. Intensity Reconstruction of Guitar Dipole Mode. Note That Most of the Energy is Produced at the Rose.

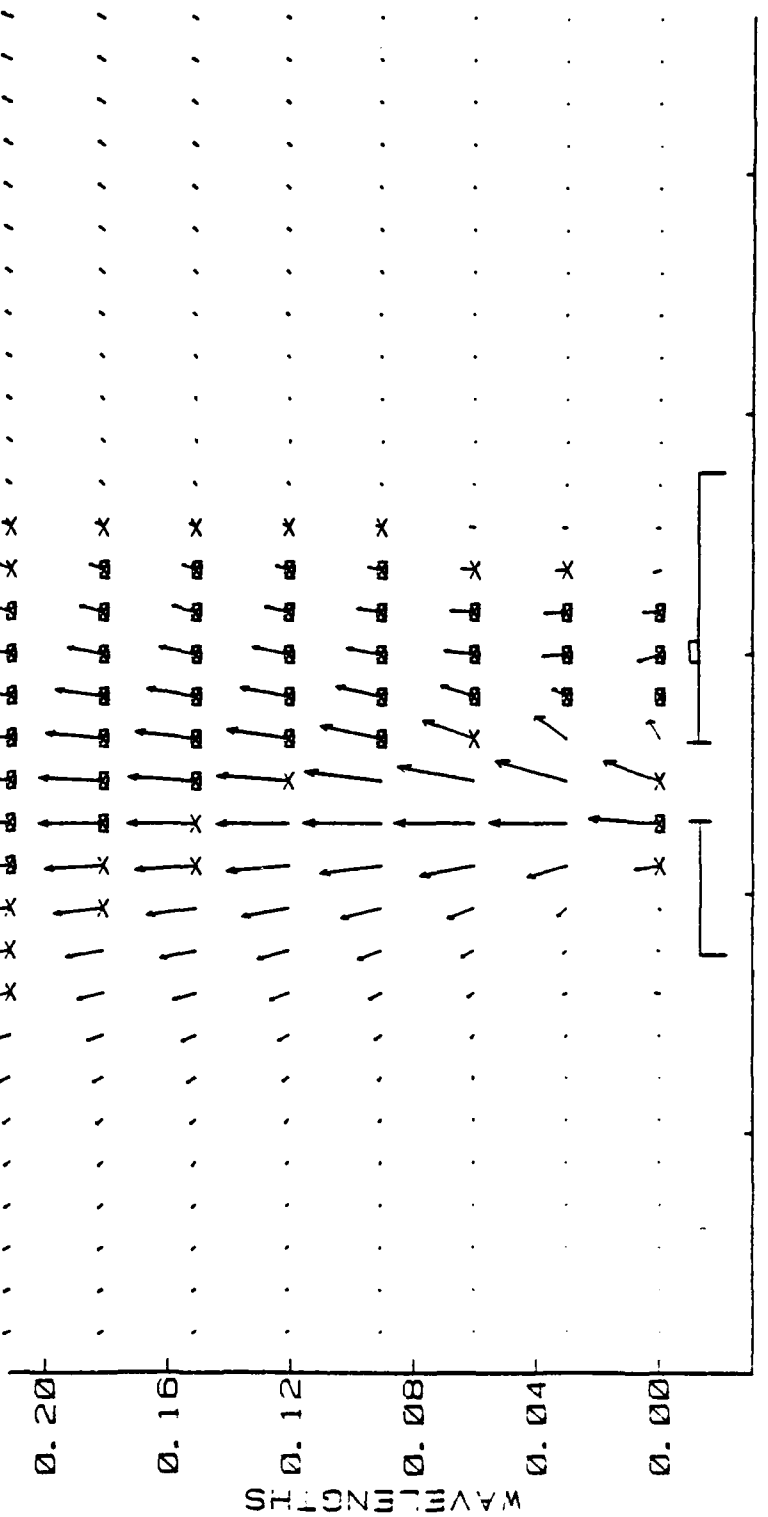

Figure 21. Energy Flow Map of Guitar Dipole Mode Taken Across Center of the Long Dimension. Note Flow Into Page Over the Bridge.

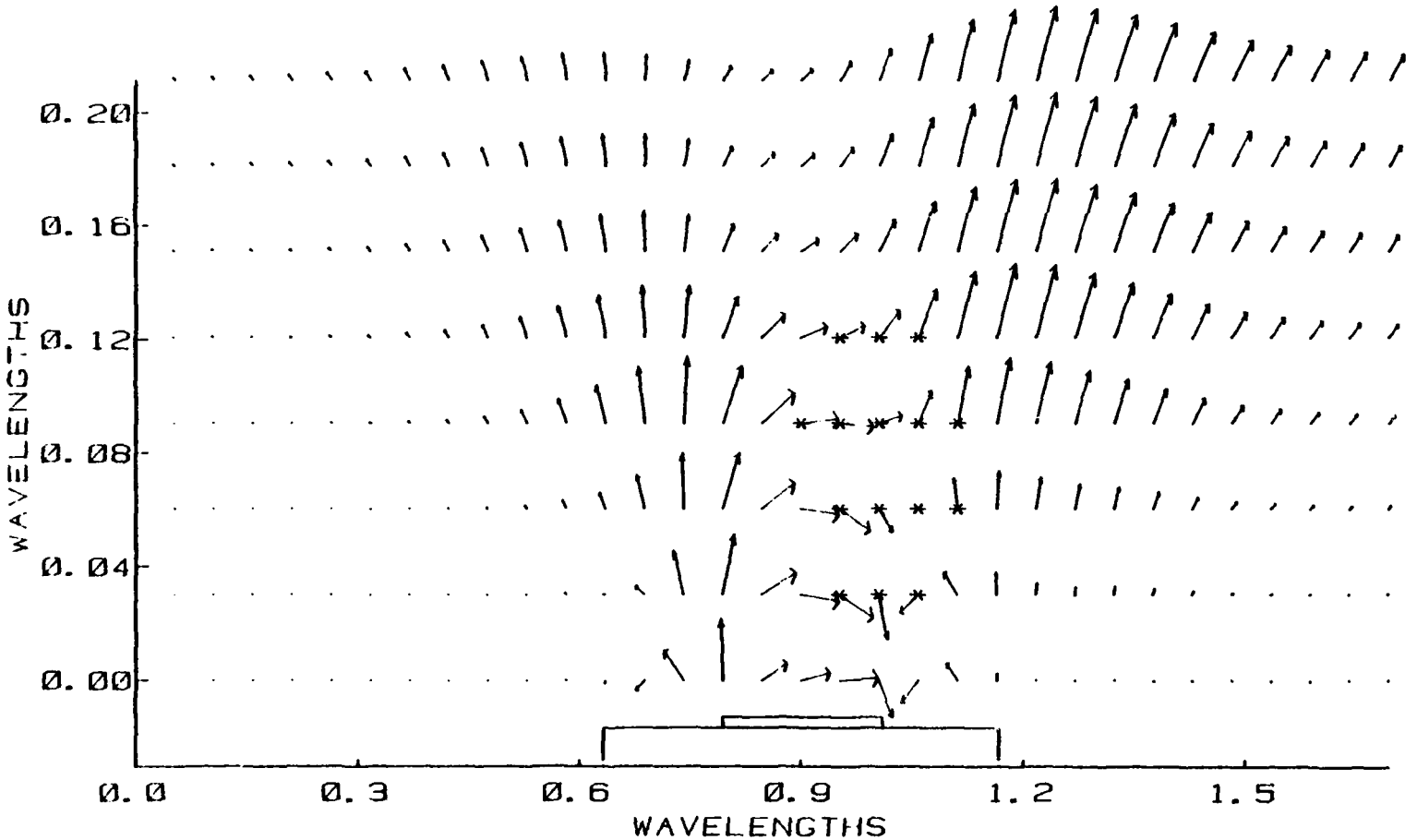

Figure 22. Energy Flow Map of Guitar Dipole Taken Across Lower Bout Through Bridge. Note That Circulating Flow Creates a Near-Field Short-Circuit.

the rose becomes very important in the study of how a guitar produces sound energy.

5.3.2 Second Study

The preliminary work indicated that the plate modes of this guitar were reasonably similar to published results on other guitars. Additionally, more information is available with this technique in that we are able to record the motion of the air as well as that of the plate. The next step was to study the guitar over a range of frequencies to observe its behavior. The frequencies chosen were those corresponding to notes available in a tuned guitar. Each string was excited at the open, fret 2, and fret 4 positions. Eighteen data files resulted covering a frequency range of 79 to 425 Hz, or the notes E_2 to G_4 sharp. The strings were clamped at frets 2 and 4 by a capo (a common guitarist's tool for raising the base tuning of the guitar). The electro-magnet was used to excite the selected string, and the other strings were damped to eliminate any sympathetic excitation.

The velocity reconstructions are shown in Figures 23 and 24. The cavity resonance for this guitar is around 100 Hz. At the cavity resonance, one would expect the guitar to be acting as a Helmholtz resonator. The air in the rose would be acting as a piston, and therefore we would expect to see this effect in our reconstructions. This is indeed the case as shown in Figure 23. But examination of the other

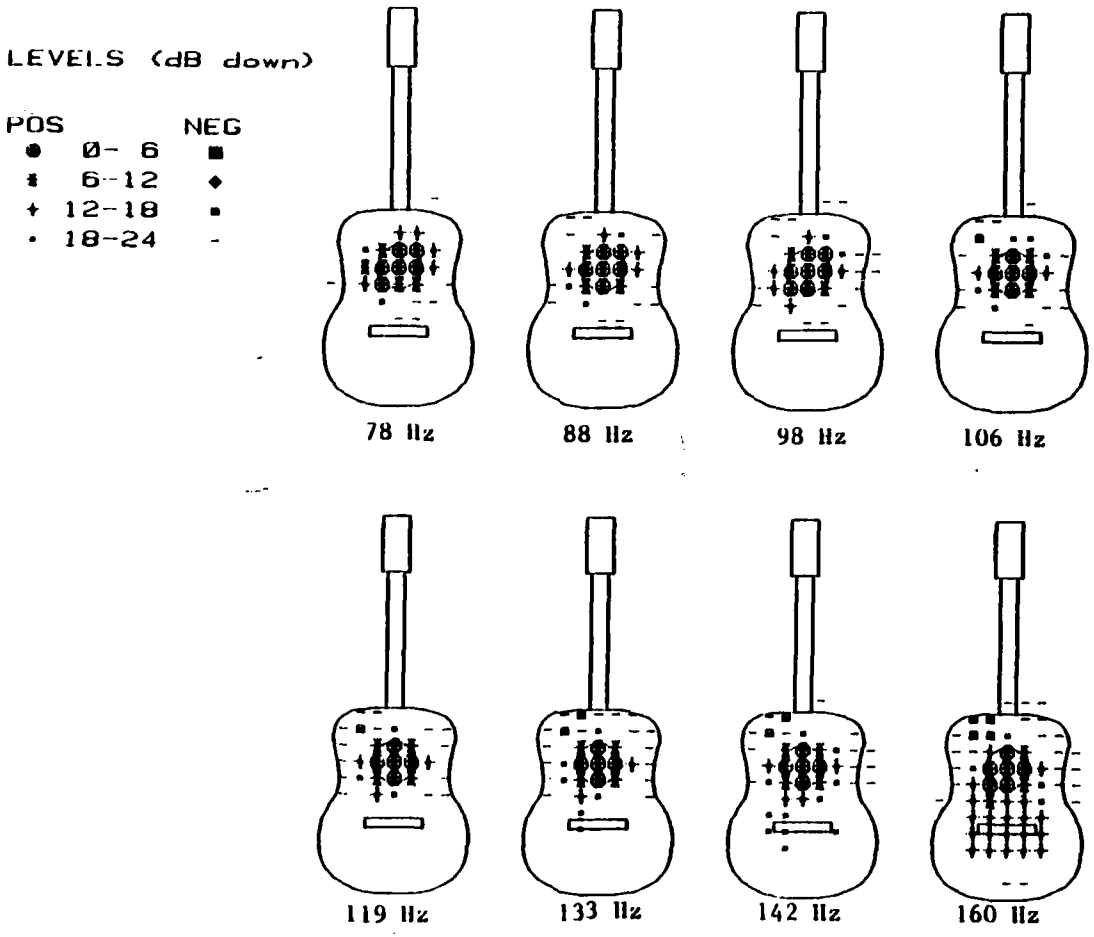

Figure 23. Multiple Velocity Reconstructions of Guitar Top Plate Over the Frequency Range 78 to 160 Hz.

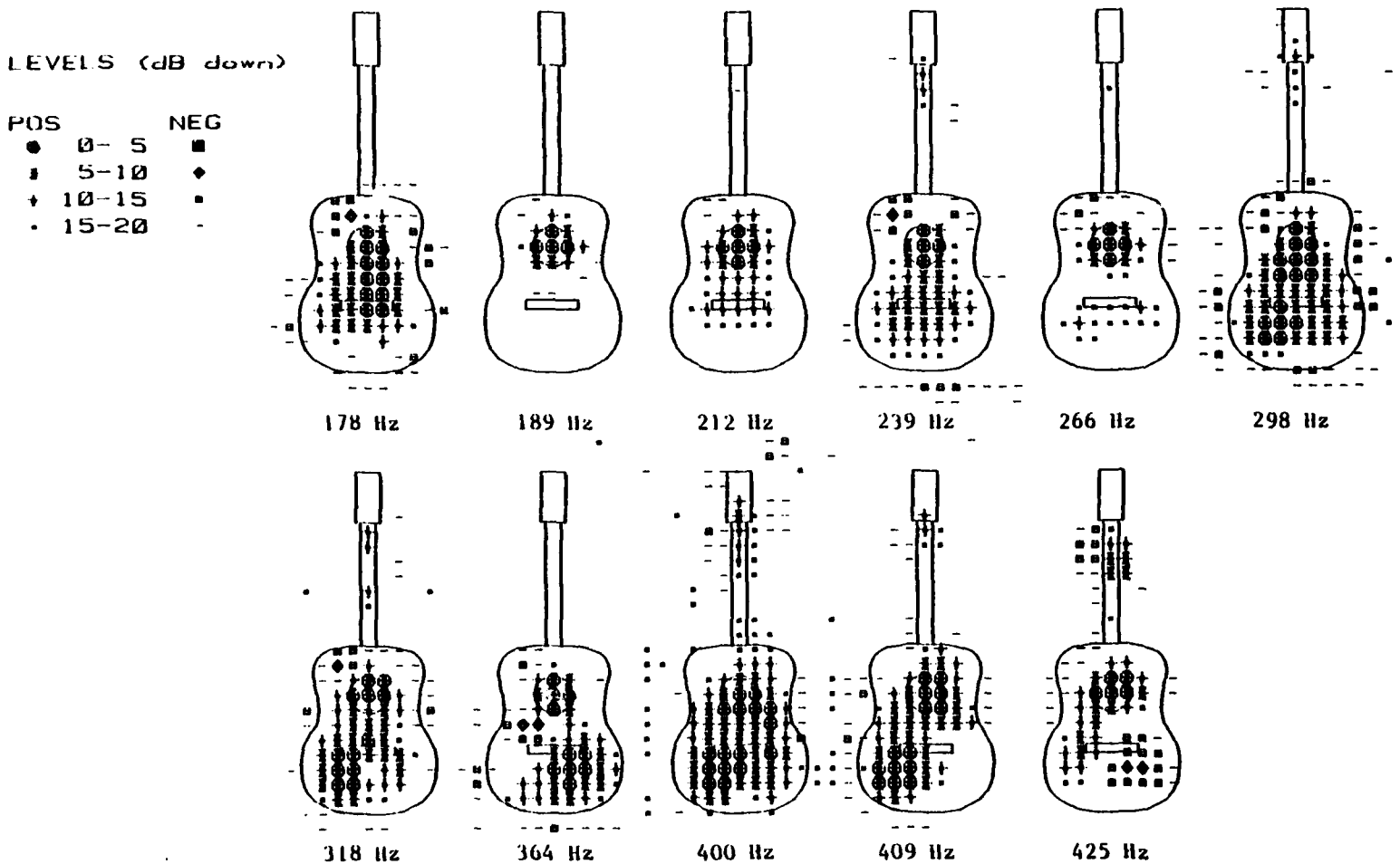

Figure 24. Continuation of Figure 23 Over the Frequency Range 178 to 425 Hz.

frequencies show that the air in the rose is always an area of large velocity over this range. This effect is missed by techniques such as interferometry. In fact, even at frequencies with large plate velocities, as at 160 Hz, the rose is still quite dominant.

The first plate resonance appears around 170 Hz and this is shown clearly in the 178 Hz case of Figure 24. But the plate resonance does not span a large frequency interval and at 189 Hz the rose is again dominant. This appears to be true up to 298 Hz, where the lower bout takes over and becomes more significant than the rose velocity. Figures 23 and 24 seem to indicate that there is more than one frequency that excites the breathing mode in an assembled, string excited guitar. The final 3 frequencies of Figure 24 nicely show the evolution of the dipole mode from a breathing mode at 400 Hz. It is also interesting to note the motion of the neck at certain frequencies in Figure 24. Subsequent accelerometer measurements confirmed that this was a real effect. This small area certainly does not contribute to the radiated sound field directly but may have some effect on the width of resonance peaks due to its coupling to the body of the guitar.

Figure 25 is a plot of the ratio of the volume velocities from the rose and the top plate over the frequency range studied. The dotted line indicates a ratio equal to 1, corresponding to equal volume flow from the rose and the top

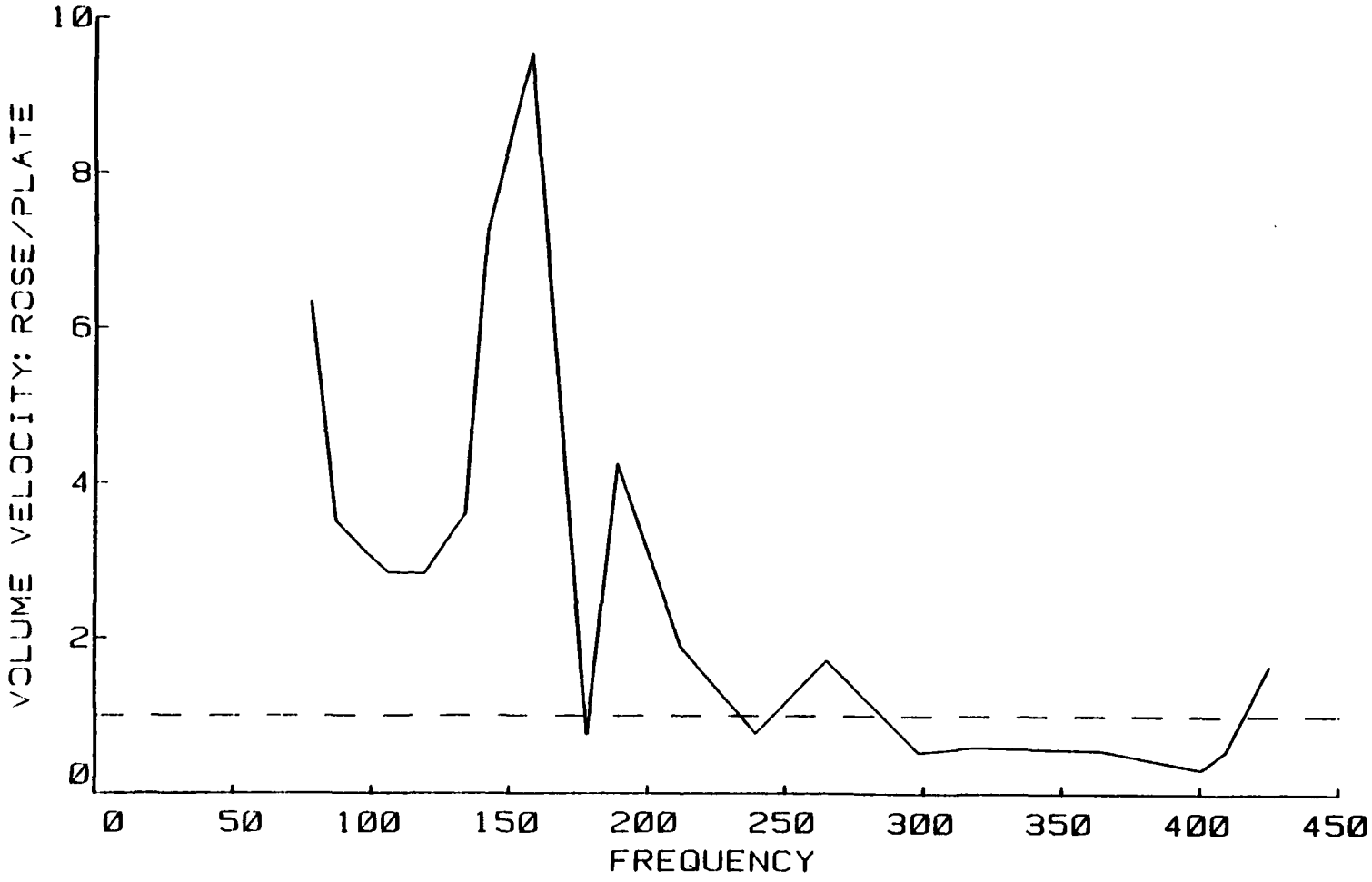

Figure 25. Plot of the Guitar Rose and Top Plate Volume Velocity Ratio versus Frequency.

plate. A ratio greater than one indicates that the rose dominates the volume flow and a ratio less than one indicates that the top plate dominates the volume flow (The volume flow is calculated by summing the velocity over that region). This plot shows that below 300 Hz, the rose is responsible for most of the volume flow produced by the guitar. Between 300 and 400 Hz the top plate becomes more significant, and at 425 Hz (the dipole mode previously discussed) the rose is again dominant. The frequencies above 400 Hz are about two octaves above the cavity resonance and this may explain the increase in activity at the rose. A study of frequencies above 425 Hz is necessary to determine whether or not the rose continues to be significant or if the top plate again dominates.

The intensity reconstructions for this study are shown in Figures 26 and 27. As with the velocity, the rose is dominant up to 266 Hz. At 189 Hz, the lower bout shows an area of negative intensity, but apparently the rose generates enough energy to produce a significant net radiation. If this negative area could be eliminated, the guitar would surely radiate better at this frequency. However, changes in the guitar that would eliminate the negative area at 189 Hz may produce problems at other frequencies. This is a complex problem in need of further study.

The intensity reconstruction at 364 Hz is interesting

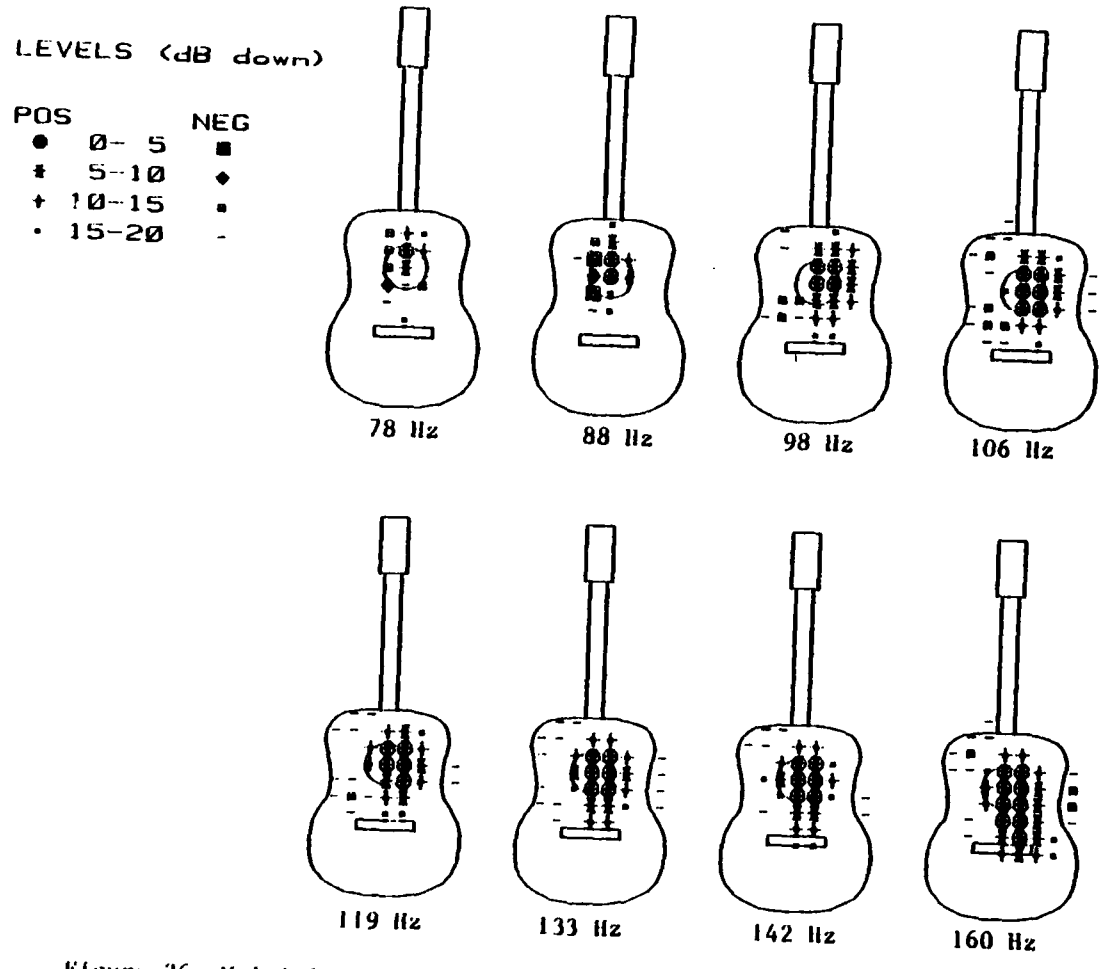

Figure 26. Multiple Intensity Reconstructions of Guitar Top Plate Over the Frequency Range 78 to 160 Hz.

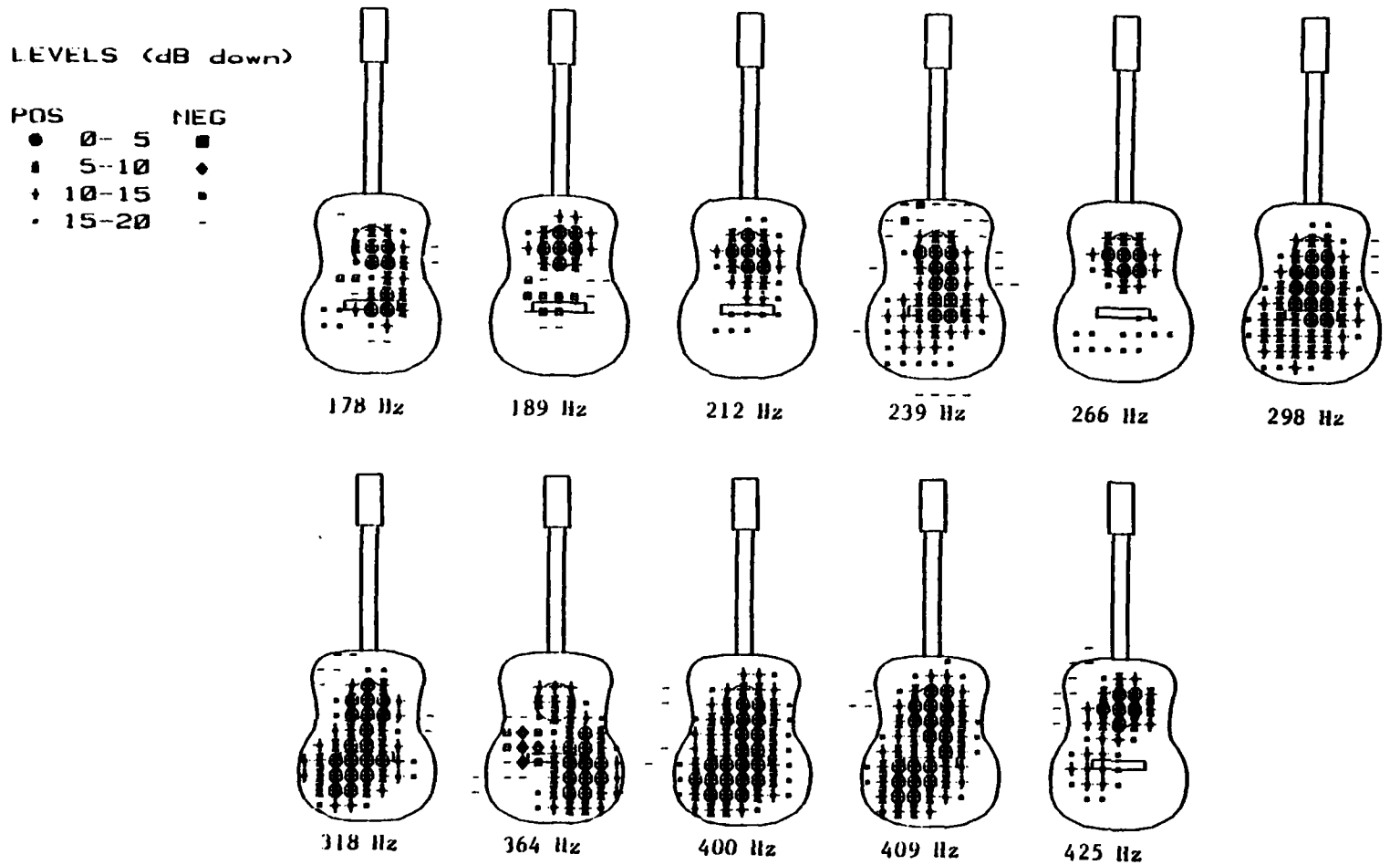

Figure 27. Continuation of Figure 26 Over the Frequency Range 178 to 425 Hz.

because the rose seems to be much less significant. The lower bout, while it has a small negative area, seems to be the energy-producing area at this frequency. Quite possibly, the rose and this negative area are acting as a nearfield short-circuit as was discussed in the first study (Time did not allow verification of this effect through energy flow mappings). If this were the case, the lower bout would be acting as the major energy producing area. This is a curious effect since at all other frequencies, the rose is a dominant area. A close study of frequencies near 364 Hz may reveal a frequency where the rose is substantially reduced in both velocity and intensity. The negative area seen at 364 Hz may expand to give another dipole mode. Evidence to support this was obtained in the preliminary study where a dipole mode without a large contribution from the rose was observed. This may be seen in Figures 28 and 29.

A plot of the ratio of the power from the rose to the power from the plate is shown in Figure 30. This plot again reflects the dominance of the rose as an energy-producing area below 300 Hz. The plate dominates between 300 and 400 Hz and the rose is again the dominant area at 425 Hz. Careful examination of the volume velocity and power ratio plots of Figure 25 and Figure 30 show that they are quite similar. The intensity seems to follow the volume flow in this guitar at frequencies below 425 Hz. This is significant because the volume flow is easier to measure

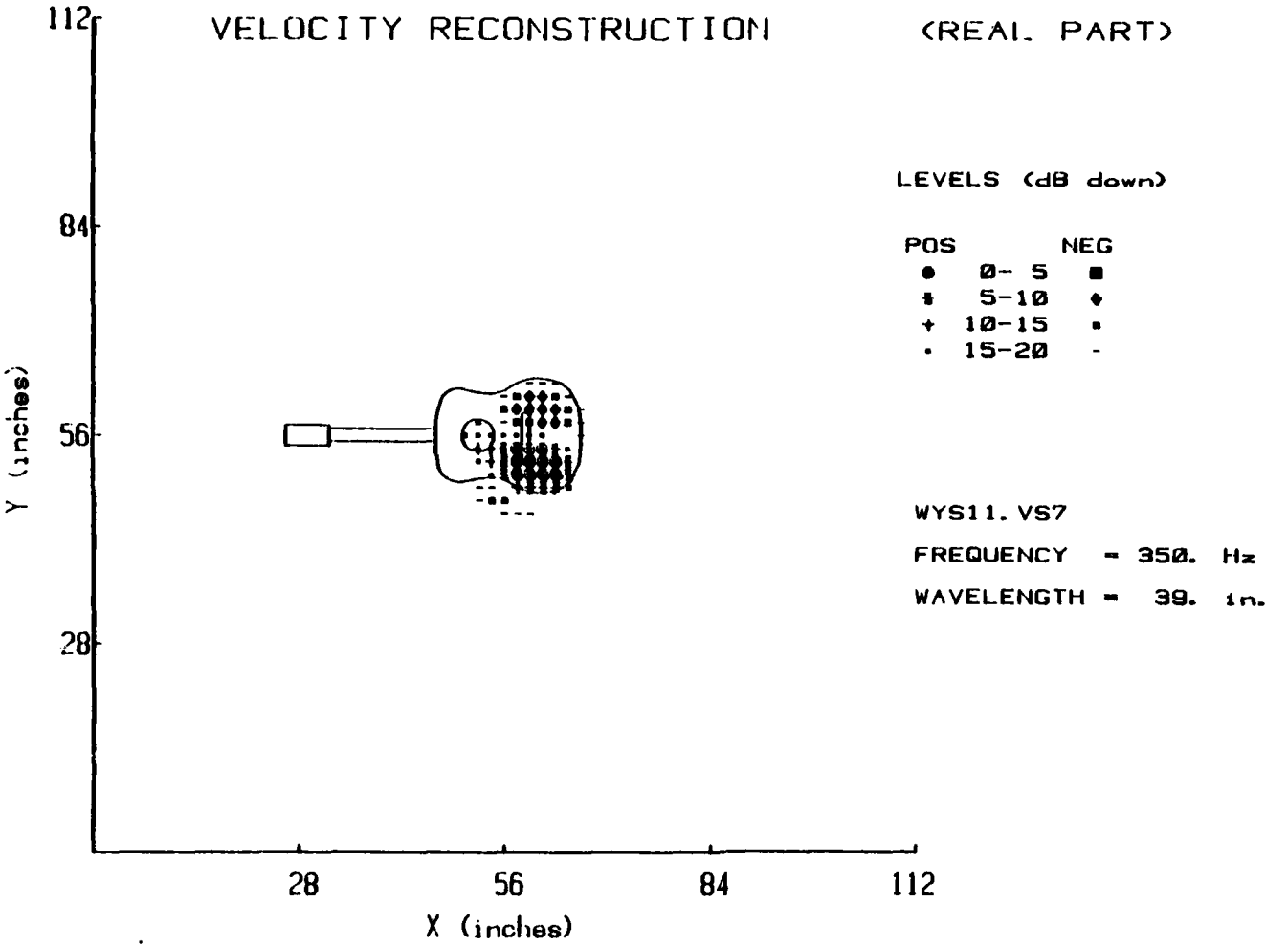

Figure 28. Velocity Reconstruction of Guitar Dipole Mode Without Activity at the Rose.

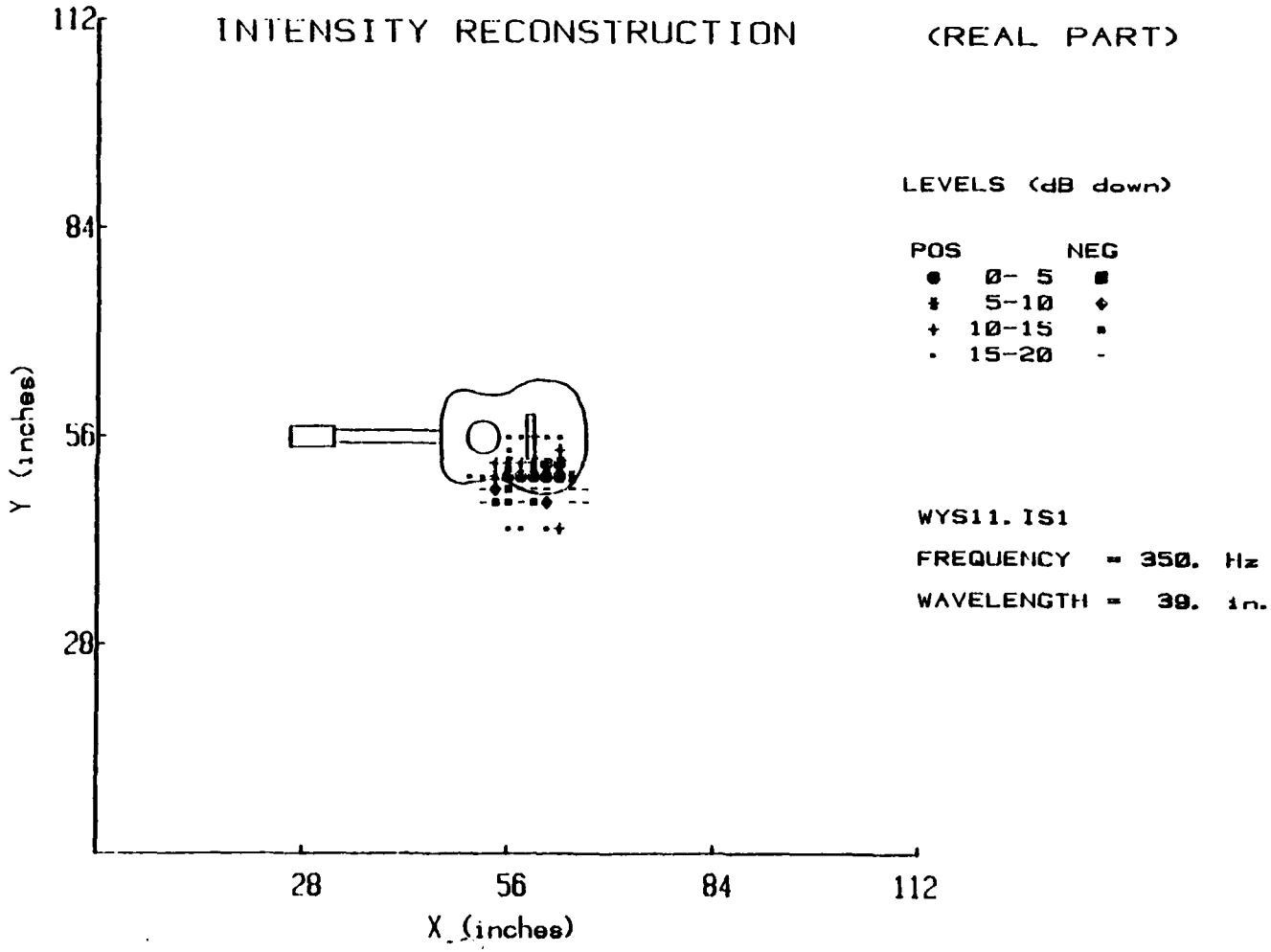

Figure 29. Intensity Reconstruction of Guitar Dipole Mode Without Energy Production at the Rose.

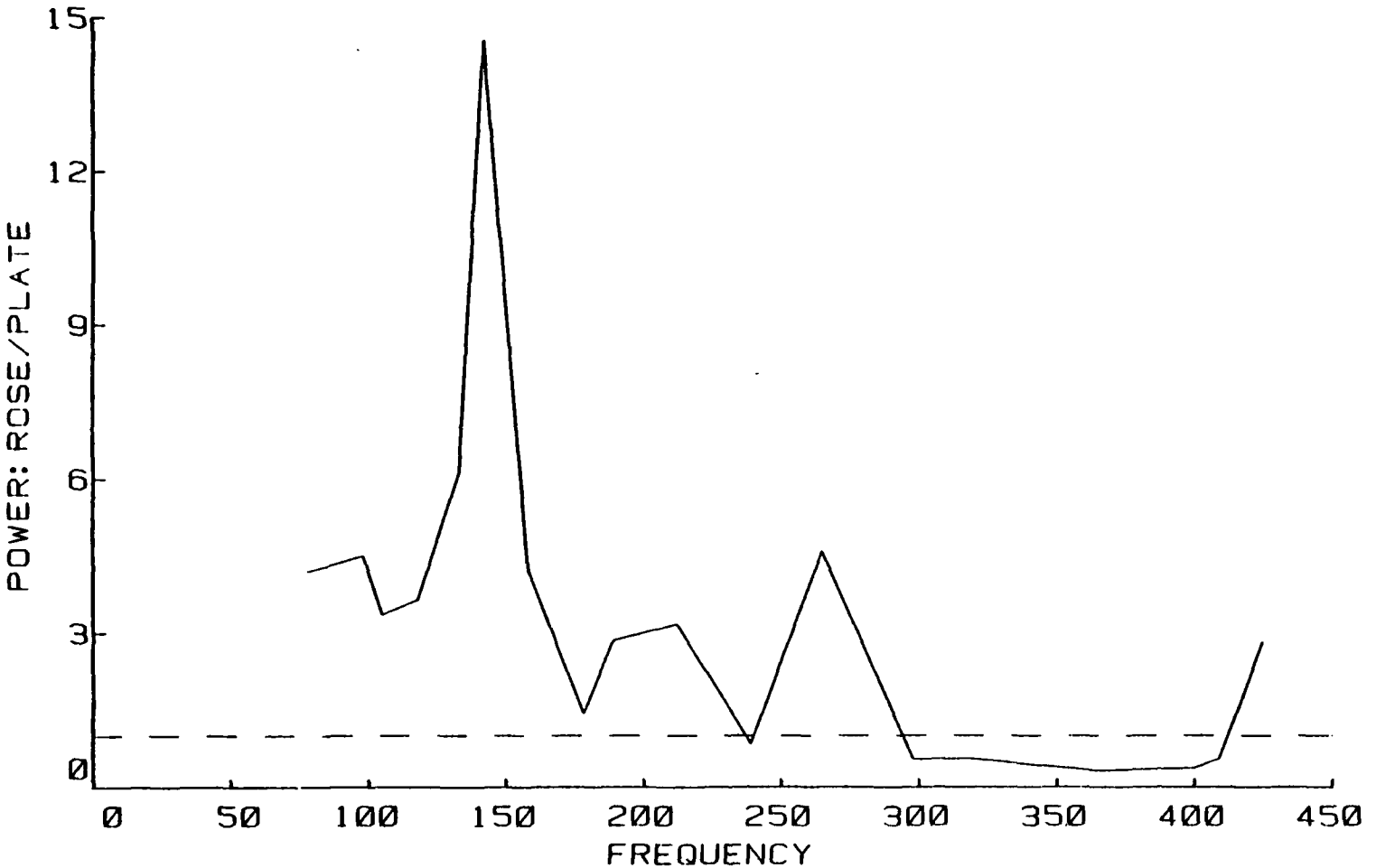

Figure 30. Plot of the Guitar Rose and Top Plate Power Ratio versus Frequency.

than the intensity. Accelerometers can determine the plate velocity, and pressure measurements at two closely spaced points perpindicular to the plane of the top plate may determine the velocity and resulting volume flow in the rose. If this were true for other guitars, it could be an easier method of finding the power produced by a guitar over this range of frequencies.

5.4 Discussion and Conclusions

Finally, the results from this study should be compared to results published by other authors. This author feels that using an intact, string-excited guitar is a more realistic approach to studying the instrument, but published results obtained with such a guitar have not been found. An understanding of the natural modes of the plates is important, but analyzing the behavior of the assembled system is necessary to better understand the instrument. The work that I would like to concentrate on is that of Caldersmith[12] and Firth[13].

The first point that I would like to address is the notion that below the cavity resonance, the guitar is a poor radiator because the motion of the air in the rose is 180^0 out of phase with the motion of the top plate. Firth[14] claims that at frequencies below the cavity resonance, the rose does not enhance the radiation of sound from the guitar and that the radiated SPL falls off at a rate of 18 dB/octave. An analogous acoustical circuit is presented to

AD-A114 777 PENNSYLVANIA STATE UNIV UNIVERSITY PARK APPLIED RESE--ETC F/G 20/1
EXPERIMENTAL METHOD TO MEASURE LOW FREQUENCY SOUND RADIATION - --ETC(U)
FEB 82 W Y STRONG N00024-79-C-6043
UNCLASSIFIED ARL/PSU/TM-82-71 NL

2 of 2

END
DATE FILMED
6-82
DTIC

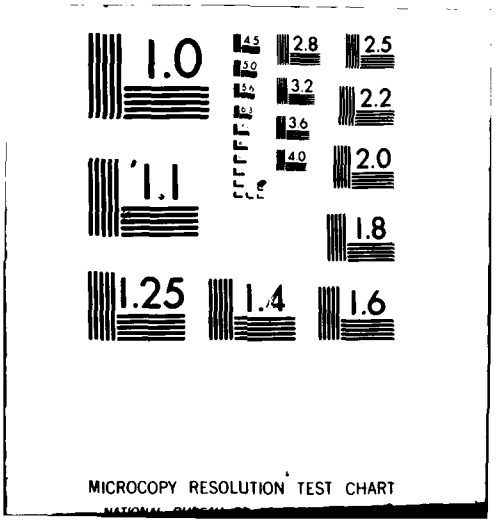
1.0
1.1
1.25
1.4
1.6
1.8
2.0
2.2
2.5
2.8
3.2
3.6
4.0
4.5
5.0
MICROCOPY RESOLUTION TEST CHART

than the intensity. Accelerometers can determine the plate velocity, and pressure measurements at two closely spaced points perpindicular to the plane of the top plate may determine the velocity and resulting volume flow in the rose. If this were true for other guitars, it could be an easier method of finding the power produced by a guitar over this range of frequencies.

5.4 Discussion and Conclusions

Finally, the results from this study should be compared to results published by other authors. This author feels that using an intact, string-excited guitar is a more realistic approach to studying the instrument, but published results obtained with such a guitar have not been found. An understanding of the natural modes of the plates is important, but analyzing the behavior of the assembled system is necessary to better understand the instrument. The work that I would like to concentrate on is that of Caldersmith[12] and Firth[13].

The first point that I would like to address is the notion that below the cavity resonance, the guitar is a poor radiator because the motion of the air in the rose is 180^0 out of phase with the motion of the top plate. Firth[14] claims that at frequencies below the cavity resonance, the rose does not enhance the radiation of sound from the guitar and that the radiated SPL falls off at a rate of 18 dB/octave. An analogous acoustical circuit is presented to

support this claim. Caldersmith[15] claims that at frequencies below the cavity resonance, air flows freely in and out of the sound hole in antiphase with the top plate motion implying a dipole effect between the rose and the top plate in support of Firth's claim.

Caldersmith models the guitar as a reflex enclosure. The body and back are represented as rigid elements with a flexable plate and sound hole on top. At low frequencies, this system is mass controlled so an inward motion of the plate compresses the air in the cavity and results in an outward flow at the rose. Caldersmith justifies the use of this model by measuring the velocity of the top and back plates of a guitar at the top plate fundamental resonance frequency. It is not surprising that the top plate motion at this frequency could be greater than the back. The conclusion drawn is that the motion of the back plate of the guitar may be ignored when studying the lower range performance of the guitar.

During the course of the second study, accelerometer measurements of the top and back plates were recorded for some frequencies to compare with the above reported results. One such data set, taken at 79 Hz, revealed that the upper and lower bout of the top plate were vibrating 180^0 out of phase resulting in a low net volume flow. But the velocity of the air in the rose was about 10 times greater than that of the top plate at this frequency. How then is this large

volume flow at the rose produced? Accelerometer measurements across the back plate revealed that the back was vibrating in phase and had an amplitude 2 to 3 times greater that the top at this frequency. This motion was found to be in phase with the air motion in the rose. Obviously this is where the large volume flow at the rose is produced. This indicates that the motion of the back plate is significant and should not be ignored. Velocity reconstructions at frequencies above and below the cavity resonance show little motion in the top plate. Therefore, we must conclude in contrast to Caldersmith and Firth, that the back plate must be a very important mechanism in the production of sound at these lower frequencies and should be considered in subsequent studies.

The second point I shall address is that of top plate modes in the guitar. It appears that the modes generally accepted to be natural modes of the top plate may occur at several frequencies in a string excited guitar. When a plate is shaker driven, one would expect a mode that is characteristic to that plate to be excited at only one frequency. This is the observed trend in shaker drive guitar plates[16, 17]. The results presented in this study of a string excited guitar indicate that these modes, or what may be slight variations of these modes, occur at more than one frequency. This leads to the conclusion that a complex relationship between the strings, ribs, body, and neck of the guitar causes similar modes at different frequencies.

Adding these elements (strings, ribs, etc.) increases the number of degrees of freedom and turns single resonances into multiplets with normal modes similar to those of the simple plate. One would think that a more or less flat response curve with many overlapping multiplets rather than a few sharp resonances would be desirable because this would eliminate any notes that sound much louder than their neighbor.

The next logical step in this research would be to study the back plate of the guitar in a manner similar to that used in the top plate study. This should lead to a better understanding of the interaction between the two plates. The development of an analogous acoustical circuit containing the back plate would certainly assist in this endeavor and should be realizable after studying the back plate. The effects of the neck being coupled to the body and its resultant vibrations are also of interest. Of course the ribbing structure is very important. There has been some work[18] in which the vibrations of the top plate of guitars with different numbers of ribs were examined. It would be interesting to study any changes in the intensity with the change in the number of ribs. Lastly, the effects of the sides of the guitar should be investigated. It seems that the sides are generally assumed to be rigid, but when the guitar is played, one can feel the sides vibrating.

A useful research team would consist of a luthier and a

scientist using nearfield holography as a research tool. The luthier's knowledge of guitar construction would allow him to make subtle changes in the guitar's construction. The effect of these changes could be studied by nearfield holography, and a better understanding of how structural changes affect radiation could be achieved. Taking a particular instrument that is considered to have superior qualities and determining its radiation characteristics over a frequency range of interest could create a 'standard of excellence'. The luthier/scientist team could endeavor to create an instrument that matched the radiation characteristics of this standard of excellence and should thereby develop an instrument of exceptional quality. In mass-produced instruments, nearfield holography could be used as a quality control tool for instruments in higher price ranges. At any rate, the holographic technique presented here could act as a major contributor to the understanding of musical instrument radiation and possibly raise the standard of quality in many applications.

REFERENCE NOTES

1. J. D. Maynard and E. G. Williams, "Nearfield Holography, a New Technique for Noise Radiation Measurement," NOISE-CON 81, Proc. Nat. Conf. Noise Control Eng., Raleigh, NC USA, 19 (1981)

2. Discussion follows E. G. Williams and J. D. Maynard, "Intensity Vector Field Mapping with Nearfield Holography," CETIM conf. on Recent Devel. in Acoustic Intensity Meas., Senlis, France, 31 (1981)

3. E. G. Williams, J. D. Maynard, and E. Skudrzyk, "Sound Source Reconstructions Using a Microphone Array," J.A.S.A. 68, 340-344 (1980)

4. E. G. Williams and J. D. Maynard, "Holographic Imaging without the Wavelength Resolution Limit," Phys. Rev. Lett. 45, 554-557 (1980)

5. Op. Cit. J. D. Maynard and E. G. Williams, "Nearfield Holography, a New Technique for Noise Radiation Measurement,"

6. E. G. Williams, Private Communication.

7. T. B. Beyer, Master's Thesis, Pennsylvania State University, (1982)

8. M. Heckl, "Schallabstrahlung Von Platten Bei Punktformiger Anregung," Acustica 9, 371-380 (1959)

9. E. V. Jansson, "A Study of Acoustical and Hologram Interferometric Measurements of the Top Plate Vibrations of a Guitar," Acustica 25, 95-100 (1971)

10. I. M. Firth, "Physics of the Guitar at the Helmholtz and First Top-Plate Resonances," J.A.S.A. 61, 588-593 (1977)

11. G. Caldersmith, "Guitar as a Reflex Enclosure," J.A.S.A. 63, 1566-1575 (1978)

12. Ibid, Caldersmith

13. Op. Cit., Firth, "Physics of the Guitar at the Helmhlotz and First Top Plate Resonances"

14. Ibid, Firth

15. Op. Cit., Caldersmith, "Guitar as a Reflex Enclosure"

16. Op. Cit., Firth, "Physics of the Guitar at the Helmholtz and First Top Plate Resonances"

17. Op. Cit., Jansson, "A Study of Acoustical and Hologram Interferomertic Measurements of the Top Plate Vibrations of a Guitar"

18. O. Jovicie and J. Jovicie, "The Role of Radial Ribs on the Resonance Board of the Guitar. II. Their Effect on the Nodal Lines of the Board (Holographic Study)," Acustica 38, 180-185 (1977)

BIBLIOGRAPHY

1. Beyer, T. B., Master's Thesis, Pennsylvania State University, (1982)

2. Caldersmith, G., "Guitar as a Reflex Enclosure," J.A.S.A. 63, 1566-1575 (1978)

3. Firth, I. M., "Physics of the Guitar at the Helmholtz and First Top-Plate Resonances," J.A.S.A. 61, 588-593 (1977)

4. Heckl, M., "Schallabstrahlung Von Platten Bei Punktformiger Anregung," Acustica 9, 371-380 (1959)

5. Jansson, E. V., "A Study of Acoustical and Hologram Interferometric Measurements of the Top Plate Vibrations of a Guitar," Acustica 25, 95-100 (1971)

6. Jovicie, O. and Jovicie, J., "The Role of Radial Ribs on the Resonance Board of the Guitar. II. Their Effect on the Nodal Lines of the Board (Holographic Study)," Acustica 38, 180-185 (1977)

7. Maynard, J. D. and Williams, E. G., "Nearfield Holography, a New Technique for Noise Radiation Measurement," NOISE-CON 81, Proc. Nat. Conf. Noise Control Eng., Raleigh, NC USA, 19 (1981)

8. Williams, E. G. and Maynard, J. D., "Holographic Imaging without the Wavelength Resolution Limit," Phys. Rev. Lett. 45, 554-557 (1980)

9. Williams, E. G. and Maynard, J. D., "Intensity Vector Field Mapping with Nearfield Holography," CETIM conf. on Recent Devel. in Acoustic Intensity Meas., Senlis, France, 31 (1981)

10. Williams, E. G., Maynard, J. D. and Skudrzyk, E., "Sound Source Reconstructions Using a Microphone Array," J.A.S.A. 68, 340-344 (1980)

DISTRIBUTION LIST FOR TM 82-71

Commander (NSEA 0342)
Naval Sea Systems Command
Department of the Navy
Washington, DC 20362

Copies 1 and 2

Commander (NSEA 9961)
Naval Sea Systems Command
Department of the Navy
Washington, DC 20362

Copies 3 and 4

Defense Technical Information Center
5010 Duke Street
Cameron Station
Alexandria, VA 22314

Copies 5 through 10